
Review

Carbon-Chain Chemistry in the Interstellar

Medium

Kotomi TANIGUCHI¹, Prasanta GORAI,² and Jonathan C. TAN^{2,3}

¹Division of Science, National Astronomical Observatory of Japan (NAOJ), National Institutes of Natural Sciences, 2-21-1 Osawa, Mitaka, Tokyo 181-8588, Japan

²Department of Space, Earth and Environment, Chalmers University of Technology, SE-412 96, Gothenburg, Sweden

³Department of Astronomy, University of Virginia, Charlottesville, VA 22904-4325, USA

*E-mail: kotomi.taniguchi@nao.ac.jp, prasanta.astro@gmail.com

Received (reception date); Accepted (acceptation date)

Abstract

The presence of carbon-chain molecules in the interstellar medium (ISM) has been known since the early 1970s and > 100 such species have been identified to date, making up > 40% of the total of detected ISM molecules. They are prevalent not only in star-forming regions in our Galaxy but also in other galaxies. These molecules provide important information on physical conditions, gas dynamics, and evolutionary stages of star-forming regions. More complex species of polycyclic aromatic hydrocarbons (PAHs) and fullerenes (C_{60} and C_{70}) have been detected in circumstellar envelopes around carbon-rich Asymptotic Giant Branch (AGB) stars and planetary nebulae, while PAHs are also known to be a widespread component of the ISM in most galaxies. Recently, two line survey projects toward the starless core Taurus Molecular Cloud-1 with large single-dish telescopes have detected many new carbon-chain species, including molecules containing benzene rings. These new findings raise fresh questions about carbon-bearing species in the Universe. This article reviews various aspects of carbon-chain molecules, including observational studies, chemical simulations, quantum calculations, and laboratory experiments, and discusses open questions and how future facilities may answer

them.

Key words: astrochemistry — ISM: molecules — ISM: abundances

1 Introduction

1.1 Brief Overview of Astrochemistry

Astrochemistry is an interdisciplinary research field concerning “study of the formation, destruction, and excitation of molecules in astronomical environments and their influence on the structure, dynamics, and evolution of astronomical objects” (Dalgarno 2008). Astrochemical studies can involve various approaches: astronomical observations; laboratory experiments on reactions and diagnostic spectroscopy; chemical simulations; and quantum chemical calculations. Collaborative studies among these approaches have been crucial in revealing the great variety of chemical pathways that operate in space.

Approximately 300 molecules have been discovered in the interstellar medium (ISM) or circumstellar envelopes (CSEs) to date (the Cologne Database for Molecular Spectroscopy (CDMS)¹; McGuire (2022)). Technical innovations and advances in observational facilities have boosted the detection of new, rarer interstellar molecules including isotopologues. These molecules have been detected in various physical conditions of the ISM; diffuse atomic H clouds ($n_{\text{H}} \approx 100 \text{ cm}^{-3}$, $T \approx 70 - 80 \text{ K}$), molecular clouds ($n_{\text{H}} \approx 10^4 \text{ cm}^{-3}$, $T \approx 10 \text{ K}$), prestellar cores² ($n_{\text{H}} \approx 10^5 - 10^6 \text{ cm}^{-3}$, $T \approx 10 \text{ K}$), protostellar cores ($n_{\text{H}} \approx 10^7 \text{ cm}^{-3}$, $T \approx 100 - 300 \text{ K}$), protoplanetary disks ($n_{\text{H}} \approx 10^4 - 10^{10} \text{ cm}^{-3}$, $T \approx 10 - 500 \text{ K}$), and envelopes of evolved stars ($n_{\text{H}} \approx 10^{10} \text{ cm}^{-3}$, $T \approx 2000 - 3500 \text{ K}$). Beyond our Galaxy, about 70 molecules have been detected in extragalactic sources.

Although 98% of the total mass of baryons consists of hydrogen (H) and helium (He), heavier trace elements such as carbon (C), oxygen (O), and nitrogen (N) are important constituent elements of interstellar molecules. These elements can make interstellar molecules complex and chemically rich. In particular, carbon composes the backbones of many molecules and is a prerequisite for organic chemistry.

Astrochemical studies of star-forming regions in our Galaxy have progressed rapidly in recent years, including in both nearby low-mass and more distant high-mass star-forming

¹ <https://cdms.astro.uni-koeln.de/classic/molecules>

² We use this term for gravitationally bound objects with central number densities above 10^5 cm^{-3} (Caselli et al. 2022).

regions. The interstellar molecules in these regions provide information on both macroscopic aspects and microscopic processes that help us to understand physical conditions and star formation histories. In the Universe, including our Galaxy, most stars form from self-gravitating molecular clouds, i.e., where hydrogen exists predominantly in the form of H_2 , mediated via formation on dust grain surfaces (Hollenbach & Salpeter 1971). In the gas phase, ion-molecule reactions, which can proceed even at cold temperatures as low as ~ 10 K, synthesize many molecules (e.g., Herbst 1983; Herbst et al. 1983, 1984). At the same time, complex organic molecules (COMs)³ begin to form mainly by hydrogenation reactions on dust grain surfaces (e.g., CH_3OH formation by successive hydrogenation reactions of CO ; Watanabe & Kouchi (2002)). During the protostellar and protoplanetary disk stage, chemical processes and chemical composition become much more complex because of stellar feedbacks, such as protostellar radiative heating via dust reprocessed infrared radiation, direct impact of energetic UV and X-ray photons and relativistic cosmic ray particles, and shock heating produced by protostellar outflows and stellar winds.

In addition to chemical composition, isotopic fractionation in some molecules can be an indicator of chemical inheritance or *in situ* chemical changes and has been subject to a variety of astrochemical studies. Especially deuterium fractionation (D/H) and nitrogen fractionation ($^{14}\text{N}/^{15}\text{N}$) are essential for helping to trace the journey of materials during star and planet formation (for reviews Caselli & Ceccarelli 2012; Jørgensen et al. 2020; Öberg & Bergin 2021). These are particularly important for revealing the formation of our Solar System (e.g., Jensen et al. 2019), one of the most fundamental questions of astronomy.

This review focuses on “carbon-chain molecules”, one of the major groups of molecules in the Universe. They are abundant in the ISM and known to be useful tracers of current physical conditions and past evolutionary history. In particular, as we will see, they can be used to probe the kinematics of chemically young gas and of the early stage of molecular clouds (e.g., Dobashi et al. 2018; Pineda et al. 2020). This means that line emission from rotational transitions of carbon-chain species is unique probes of gas kinematics related to star formation. Some carbon-chain species have been suggested to possess the potential to form COMs or more complex molecules that are related to biologically relevant molecules including amino acids. For example, cyanoacetylene (HC_3N) has been suggested to be a candidate for the precursor of Cytosine, Uracil, and Thymine (Choe 2021). These aspects further motivate us to study their chemical characteristics in the Universe.

³ Molecules consisting of more than 6 atoms (Herbst & van Dishoeck 2009).

1.2 History of Studies of Carbon-Chain Molecules

Carbon-chain molecules are one of the major constituents of molecules detected in the Universe (see section 2.3). After the discovery of the first carbon-chain molecules in the ISM in the 1970s, many efforts to explain their formation routes were made by laboratory experiments and chemical simulations in the 1980s. In the beginning, the focus was on gas-phase chemical reactions of small species (Prasad & Huntress 1980a, 1980b; Graedel et al. 1982). Herbst (1983) was able to reproduce the observed abundance of a larger species, C_4H , in Taurus Molecular Cloud-1 (TMC-1; $d \approx 140$ pc), which is one of the most carbon-chain-rich sources. Herbst (1983) found that ion-molecule reactions with a large amount of atomic carbon (with its abundance of $\sim 10^{-5}$) are necessary to explain the observed C_4H abundance. Suzuki (1983) found that reactions including C^+ can also play essential roles in carbon-chain growth. These results suggested that carbon-chain species could efficiently form in young molecular clouds before carbon is locked into CO molecules.

In the 1990s, carbon-chain molecules were detected in many molecular clouds, beyond the previously well-studied examples, such as TMC-1. Survey observations revealed that carbon-chain molecules are evolutionary indicators of starless and star-forming cores in low-mass star-forming regions; they are abundant in starless cores (Suzuki et al. 1992; Benson et al. 1998). These studies reinforced the view that these molecules are formed from ionic (C^+) or atomic (C) carbon in the early stages of molecular clouds, before CO formation, as predicted by chemical simulations. Figure 1 shows the carbon-chain growth and formation pathways of nitrogen- and sulfur-bearing species (HC_3N , HC_5N , and CCS), which have been frequently detected in low-mass starless cores in the early stages of molecular cloud cores. These reaction schemes are constructed from results of the latest chemical simulations with a constant temperature of 10 K and a constant density of $n_H = 10^4 \text{ cm}^{-3}$ in $t < 10^4$ yr (Taniguchi et al. 2019b). Hydrocarbons can form efficiently from C^+ and C via ion-molecule reactions involving H_2 and dissociative recombination reactions leading to the formation of neutral hydrocarbons. Such carbon-chain formation in cold molecular clouds is basically consistent with that proposed in the 1980s.

During the later stages of starless cores, carbon-chain species are adsorbed onto dust grains or destroyed by reactions with ions such as He^+ and H^+ , and reactions with atomic oxygen (O). These processes result in the depletion of carbon-chain species by the later stages of prestellar cores and protostellar cores. Thus, carbon-chain molecules were classically known as “early-type species”.

Subsequent studies found that carbon-chain species exist in lukewarm regions ($T \approx$

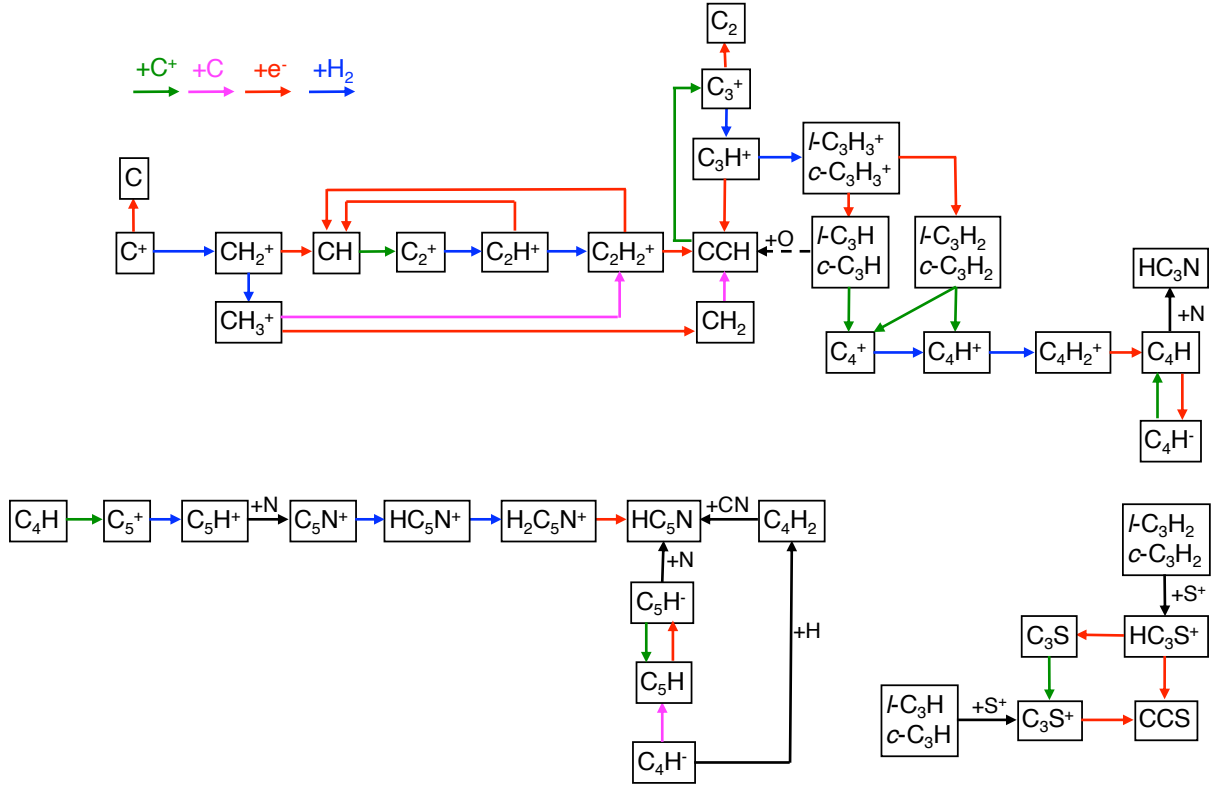


Fig. 1 Carbon-chain growth (for number of C ≤ 4) and formation processes of HC₅N and CCS in early stages of molecular clouds ($t < 10^4$ yr). The dashed arrow from *l,c*-C₃H to CCH indicates that this reaction is important around 10^5 yr.

25 – 35 K) around low-mass protostars, and a new carbon-chain formation mechanism starting from CH₄ was proposed (see section 2.4). This was named Warm Carbon-Chain Chemistry (WCCC) (for a review Sakai & Yamamoto 2013). More recently, carbon-chain chemistry around massive young stellar objects (MYSOs) has been explored (section 2.5), and Hot Carbon-Chain Chemistry (HCCC) has been proposed (Taniguchi et al. 2023).

Furthermore, very complex carbon-chain species, branched-chain molecules, and molecules including benzene rings have been discovered in the ISM in the last few years (section 3.1.1). These new findings bring fresh challenges and excite our curiosity for a deeper understanding of carbon-chain chemistry in the ISM.

1.3 Outline of This Review

In this review article, we summarize results from studies of carbon-chain molecules by astronomical observations, chemical simulations, quantum chemical calculations, and laboratory

experiments. In section 2, we overview the current status of the detected carbon-chain species in the ISM and the main concepts of carbon-chain chemistry around protostars. We review observational studies (section 3), chemical models (section 4), quantum chemical calculations (section 5), and laboratory experiments (section 6). Finally, we list current open and key questions regarding carbon-chain species and summarise in section 7.

Here, we set a definition of “carbon-chain molecules” for this review article, as recent detections of new interstellar species complicate this categorization. We include linear carbon-chain species with more than two carbon atoms and cyclic species with more than three carbon atoms containing at least one double ($=$) or triple (\equiv) bond as carbon-chain molecules. Even if molecules meet the above criteria, species containing functional groups related to organic chemistry (e.g., $-\text{OH}$, $-\text{NH}_2$) are excluded from carbon-chain molecules, because they are generally categorized as COMs. As an exception, *cyclic*- C_2Si , which consists of a cyclic structure with two carbon atoms and one Si atom, is treated as a carbon-chain species. In addition to straight linear carbon-chain species, we also treat branched carbon-chain species (e.g., iso-propyl cyanide) as carbon-chain molecules. Molecules containing the structure of benzene, polycyclic aromatic hydrocarbons (PAHs), and fullerenes (C_{60} or C_{70}) are also included. In the following sections, we abbreviate *linear*- and *cyclic*- as *l*- and *c*-, if necessary to indicate the molecular structure (e.g., *l*- C_3H_2 and *c*- C_3H_2). This review article summarizes literature results until the end of December 2022.

2 Development of Carbon-Chain Chemistry

2.1 Detection of Carbon-Chain Species in the ISM and CSEs

Cyanoacetylene (HC_3N), the shortest cyanopolyynes (HC_{2n+1}N), was the first carbon-chain molecule detected in space. It was found toward a high-mass star-forming complex, Sagittarius B2 (Sgr B2; Turner 1971). Following this, two molecules from hydrocarbon family, CH_3CCH (Buhl & Snyder 1973) and C_2H (Tucker et al. 1974), were detected. The next higher-order cyanopolyynes, cyanodiacetylene (HC_5N), was identified toward Sgr B2, i.e., the same region where HC_3N was first observed (Avery et al. 1976). In the following year, C_2 was detected toward Cygnus OB2 No.12 via electronic spectra (Souza & Lutz 1977).

Observations of carbon-chain species are also expanded to other star-forming regions and HC_3N was detected toward various types of sources. For instance, it was identified toward Heiles cloud 2 (TMC-1 ridge is a part of the Heiles cloud) (Morris et al. 1976), and HC_5N was found to be abundant in the same region (Little et al. 1977). The detections of the higher-order

cyanopolyynes, HC_7N , and HC_9N , were also reported toward TMC-1 (Kroto et al. 1978; Broten et al. 1978). Around the same time, C_3N , C_4H , and CH_3CCH were found toward dark clouds, including TMC-1 (Friberg et al. 1980; Guelin et al. 1978; Irvine et al. 1981). The discoveries of several carbon-chain species in the ISM brought curiosity and opened a new field to be investigated further.

In the 1980s, several carbon-chain species were discovered in the ISM; e.g., C_3O (Matthews et al. 1984), C_3N (Guelin & Thaddeus 1977), C_3H (Thaddeus et al. 1985a), C_3S (Kaifu et al. 1987; Yamamoto et al. 1987), C_5H (Cernicharo et al. 1986), C_6H (Suzuki et al. 1986), $c\text{-C}_3\text{H}_2$ (Thaddeus et al. 1985b), $c\text{-C}_3\text{H}$ (Yamamoto et al. 1987), C_2S (Yamamoto et al. 1987), and C_3S (Kaifu et al. 1987). In the same period, two bare carbon chains, C_3 and C_5 , were identified toward IRC+10216 (Hinkle et al. 1988; Bernath et al. 1989) via their rotational-vibrational spectra.

It was noted that while many carbon-chain molecules are found to be abundant in the starless core TMC-1, some other quiescent starless cores in the Taurus region are deficient in these species. And, more generally, carbon-chain molecules have low abundances in diffuse clouds, translucent clouds, and dense hot gas around protostars, namely hot molecular cores (HMCs).

In the 1990s, there were first detection reported of C_2O (Ohishi et al. 1991), HC_2N (Guelin & Cernicharo 1991), C_7H (Guelin et al. 1997), C_8H (Cernicharo & Guelin 1996), H_2C_6 (Langer et al. 1997), C_5N (Guelin et al. 1998), $c\text{-SiC}_3$ (Apponi et al. 1999), and HC_3NH^+ (Kawaguchi et al. 1994).

In the 2000s, several complex carbon-chain molecules including linear and cyclic structures were detected: HC_4N (Cernicharo et al. 2004); $\text{CH}_3\text{C}_5\text{N}$ (Snyder et al. 2006); $c\text{-H}_2\text{C}_3\text{O}$ (Hollis et al. 2006); $\text{CH}_3\text{C}_6\text{H}$ (Remijan et al. 2006). The first and only phosphorus-bearing chain, CCP, was discovered from IRC+10216 (Halfen et al. 2008). The benzene (C_6H_6) and two polyacetylene chains, C_4H_2 and C_6H_2 , were detected with the Infrared Space Observatory (ISO; Cernicharo et al. 2001). Not only neutral carbon-chain species but also various carbon-chain anions were discovered in space. The first interstellar anion is C_6H^- , which was identified in both the circumstellar envelope IRC+10216 and the molecular cloud TMC-1 (McCarthy et al. 2006). Subsequently, C_4H^- (Cernicharo et al. 2007) and C_8H^- (Brünken et al. 2007; Remijan et al. 2007) were detected toward the same target. Two nitrogen-bearing carbon-chain anions, C_3N^- (Thaddeus et al. 2008) and C_5N^- (Cernicharo et al. 2008) were discovered in IRC+10216.

In the 2010s, we came to know about the existence of cosmic fullerenes, C_{60} and C_{70} , in

a peculiar planetary nebula with an extremely hydrogen-poor dust formation zone (Cami et al. 2010). Two diffuse interstellar bands at 9632 Å and 9577 Å were detected in the ISM and suggested to come from the C_{60}^+ ion (Foing & Ehrenfreund 1994). Campbell et al. (2015) conducted laboratory experiments of C_{60}^+ and confirmed that the diffuse interstellar bands at these two wavelengths arise from C_{60}^+ . This brought great attention to astronomers, experimentalists, theoreticians, modelers, and other scientific communities. Several other interesting carbon-chain species were detected: *l*- C_3H^+ (Pety et al. 2012); C_5S (Agúndez et al. 2014); CCN (Anderson & Ziurys 2014); carbon-chain radicals containing an oxygen atom, HC_2O (Agúndez et al. 2015), HC_5O (McGuire et al. 2017) and HC_7O (Cordiner et al. 2017); simplest nitrogen-bearing aromatic molecule, *c*- C_6H_5CN (McGuire et al. 2018); and metal-containing carbon chains, MgC_3N and MgC_4H (Cernicharo et al. 2019).

In the 2020s, two line survey programs, GOTHAM (using the 100m diameter GBT) and QUIJOTE (using the Yebes 40m telescope) focusing on TMC-1, have discovered many new carbon-chain species: $HC_{11}N$ (Loomis et al. 2021); HC_5NH^+ (Marcelino et al. 2020); HC_3O (Cernicharo et al. 2020b); C_5O (Cernicharo et al. 2021a); HC_3O^+ (Cernicharo et al. 2020b); *c*- C_5H (Cernicharo et al. 2022b); C_5H^+ (Cernicharo et al. 2022b); C_4S (Cernicharo et al. 2021f); HC_3S^+ (Cernicharo et al. 2021e); HCCS (Cernicharo et al. 2021e); HC_4S (Fuentetaja et al. 2022b); $HCCS^+$ (Cabezas et al. 2022b); HC_7NH^+ (Cabezas et al. 2022a); aromatic molecules, which include benzene ring(s), and their precursors. These newly detected species have dramatically changed the list of known interstellar molecules/carbon-chain species and brought many open questions (see section 3.1.1).

2.2 Different carbon-chain families and their present status

All of the carbon-chain species belonging to the various groups, C_n , C_nH , C_nH^- , C_nO , C_nN , C_nN^- , C_nS , C_nP , $HC_{2n+1}N$, $HC_{2n}N$, HC_nO , HC_nS , HC_nH , MgC_nH , MgC_nN , are summarized in table 1. Here information is given on their electronic ground state, electric polarizability, electric dipole moment, and present astronomical status.

Table 1. Ground state, polarizability, dipole moment and present astronomical status of different carbon chain species

Species	Ground State	Polarizability (α in \AA^3)	Dipole moment (Debye)	Detection Status		
				ISM	TMC-1	IRC+10216
C ₂	singlet	5.07 ^a	0.0	✓		✓
C ₃	singlet	5.18 ^a	0.0	✓		✓
C ₄	singlet	7.51 ^a	0.0			
C ₅	singlet	11.16 ^a	0.0	✓		✓
C ₆	singlet	14.32 ^a	0.0			
C ₇	singlet	20.50 ^a	0.0			
C ₈	singlet	23.96 ^a	0.0			
C ₉	singlet	33.36 ^a	0.0			
C ₁₀	singlet	37.70 ^a	0.0			
C _n H						
C ₂ H	doublet	4.42 ^a	0.81 ^a	✓	✓	✓
<i>l</i> -C ₃ H	doublet	5.36 ^a	3.52 ^a	✓	✓	✓
<i>c</i> -C ₃ H	doublet	4.80 ^a	2.60 ^a	✓	✓	
C ₃ H ⁺	singlet	3.69 [*]	3.00 ^b	✓	✓	
C ₄ H	doublet	7.15 ^a	2.40 ^c	✓	✓	✓
C ₄ H ⁻	singlet	9.57 [*]	5.9 ^d	✓	✓	✓
C ₅ H	doublet	10.50 ^a	4.84 ^a	✓	✓	✓
C ₅ H ⁺	singlet	8.44 [*]	2.88 ^e	✓	✓	
<i>c</i> -C ₅ H	doublet	8.77 [*]	3.39 ^f	✓		
C ₆ H	doublet	13.68 ^a	5.6 ^a	✓	✓	✓
C ₆ H ⁻	singlet	15.74 [*]	8.2 ^d	✓	✓	✓
C ₇ H	doublet	17.37 ^a	5.83 ^a	✓	✓	✓
C ₈ H	doublet	21.85 ^a	6.43 ^a	✓	✓	✓
C ₈ H ⁻	singlet	24.39 [*]	11.9 ⁵	✓	✓	✓
C ₉ H	doublet	26.38 ^a	6.49 ^a			
✓ C ₁₀ H	singlet	31.05 ^a	7.13 ^a			
<i>l</i> -C ₃ H ₂	singlet	5.61 ^a	4.10 ^a	✓	✓	
HC _n H						
HC ₂ H	singlet	3.38 ^a	0.0	✓		✓
HC ₃ H	triplet	2.58 ^a	0.51 ^g			
HC ₄ H	singlet	7.05	0.0	✓		✓
HC ₅ H	triplet	–	–			
HC ₆ H	singlet	11.95 ^a	0.0	✓		✓
HC ₇ H	triplet	–	–			
HC ₈ H	singlet	18.59 ^a	0.0			
C _n O						
C ₂ O	triplet	4.09 ^a	1.43 ^a	✓	✓	✓

Table 1 (cont'd)

Species	Ground State	Polarizability (α in \AA^3)	Dipole moment (Debye)	Detection Status		
				ISM	TMC-1	IRC+10216
C ₃ O	singlet	6.03 ^a	2.39 ^h	✓	✓	✓
HC ₃ O ⁺	singlet	–	3.41 ⁱ	✓	✓	
C ₄ O	triplet	9.21 ^a	3.01 ^j			
C ₅ O	singlet	10.93 [*]	4.06 ^k	✓	✓	✓
C ₆ O	triplet	15.41 [*]	4.88 ^j			
C ₇ O	singlet	19.51 [*]	4.67 ^l			
C ₈ O	triplet	25.99 [*]	4.80 ^l			
C _n S						
C ₂ S	triplet	6.87 ^a	3.12 ^a	✓	✓	✓
HC ₂ S ⁺	triplet		2.29 ^{l1}	✓	✓	
C ₃ S	singlet	9.65 ^a	3.939 ^a	✓	✓	✓
HC ₃ S ⁺	singlet	–	1.73 ^d	✓	✓	
C ₄ S	triplet	13.70 ^a	4.62 ^a	✓	✓	✓
C ₅ S	singlet	15.79 [*]	4.65 ^m	✓	✓	✓
C ₆ S	triplet	21.53 [*]	5.40 ^l			
C ₇ S	singlet	26.44 [*]	6.17 ^l			
C ₈ S	triplet	34.54 [*]	6.50 ^l			
C _n N						
C ₂ N	doublet	4.27 ^a	0.60 ^a	✓		✓
C ₃ N	doublet	5.68 ^a	2.86 ^a	✓	✓	✓
C ₃ N [–]	singlet	7.58 [*]	3.1 ⁿ	✓	✓	✓
C ₄ N	doublet	8.75 ^a	0.06 ^a			
C ₅ N	doublet	9.43 ^a	3.33 ^a	✓	✓	✓
C ₅ N [–]	singlet	13.26 [*]	5.20 ^o	✓	✓	✓
C ₆ N	doublet	14.91 [*]	0.21 ^p			
C ₇ N	doublet	18.95 ^a	0.87 ^a			
C ₈ N	doublet	24.16 [*]	–			
C _n P						
C ₂ P	doublet	7.52 ^a	3.24 ^a	✓		✓
C ₃ P	doublet	10.50 ^a	3.89 ^a			
C ₄ P	doublet	12.76 ^a	4.19 ^a			
C ₅ P	doublet	17.22 [*]	–			
C ₆ P	doublet	22.13 [*]	–			
C ₇ P	doublet	27.90 [*]	–			
C ₈ P	doublet	34.41 [*]	–			
HC _{2n} N						
HC ₂ N	triplet		3.30 ^q	✓		✓

Table 1 (cont'd)

Species	Ground State	Polarizability (α in \AA^3)	Dipole moment (Debye)	Detection Status		
				ISM	TMC-1	IRC+10216
HC ₄ N	triplet	8.84 ^a	4.30 ^a	✓		✓
HC ₆ N	triplet	15.07 ^a	4.89 ^a			
HC ₈ N	triplet	22.96 ^a	5.57 ^a			
HC _{2n+1} N						
HC ₃ N	singlet	5.85 ^a	3.78 ^a	✓	✓	✓
HNC ₃	singlet	6.41 [*]	6.46 ^p	✓	✓	✓
HC ₃ NH ⁺	singlet	4.90 [*]	1.87 ^r	✓	✓	
HC ₅ N	singlet	10.42 ^a	4.41 ^a	✓	✓	✓
HC ₅ NH ⁺	singlet	10.67 [*]	3.26 ^{m1}	✓	✓	
HC ₇ N	singlet	16.69 ^a	4.90 ^a	✓	✓	✓
HC ₇ NH ⁺	singlet	–	6.40 ^{o1}	✓	✓	
HC ₉ N	singlet	23.89 ^a	5.29 ^a	✓	✓	✓
HC ₁₁ N	singlet	–	5.47	✓	✓	
HC _n O						
HC ₂ O	doublet	4.20 ^c	1.8 ^s	✓	✓	
HC ₃ O	doublet	5.20 ^c	2.74 ^s	✓	✓	
HC ₄ O	doublet	7.83 [*]	2.64 ^{m1}			
HC ₅ O	doublet	10.87 [*]	2.16 ^{m1}	✓	✓	
HC ₆ O	doublet	14.46 [*]	2.11 ^{m1}			
HC ₇ O	doublet	–	2.17 ^{m1}	✓	✓	
HC ₈ O	doublet	–	2.19 ^{m1}			
HC _n S						
HC ₂ S	doublet	6.92 ^s	1.36 ^s	✓	✓	
HC ₃ S	doublet	9.62 ^s	1.28 ^s			
HC ₄ S	doublet	11.60 [*]	1.45 ^{p1}	✓	✓	
HC ₅ S	doublet	–	1.92 ^{q1}			
HC ₆ S	doublet	19.86 [*]	2.75 ^{r1}			
HC ₇ S	doublet	–	2.10 ^{q1}			
HC ₈ S	doublet	–	3.21 ^{r1}			
MetalContaining						
MgC ₂ H	doublet	10.44 [*]	1.68 ^t	✓		✓
MgC ₄ H	doublet	15.01 [*]	2.12 ^u	✓		✓
MgC ₃ N	doublet	13.16 [*]	6.30 ^u	✓		✓
MgC ₅ N	doublet	19.22	7.30 ^v	✓		✓
MgC ₆ H	doublet	21.54 [*]	2.50 ^v	✓		✓
<i>c</i> -C ₂ Si	doublet	6.79 ^a	2.4 ^a	✓		✓
<i>c</i> -C ₃ Si	singlet	11.90 ^a	4.1 ^a	✓		✓

2.2.1 Pure carbon chains - C_n

All pure linear carbon-chain species are indicated as C_n ($n > 1$). The electronic ground state of all these species is singlet, and they do not have a permanent dipole moment (see table 1). Hence, they do not show rotational transitions, and so are not detectable via rotational transitions using radio observations. Instead, they show emission in the infrared domain through their rotational-vibrational transitions, and so far three chains ($n = 2, 3, 5$) are astronomically detected from this group (see section 2.1). In diffuse and translucent environments, C_2 formation starts with the reaction of $C^+ + CH \rightarrow C_2^+ + H$, followed by a series of hydrogen abstraction reactions and dissociative recombination reactions that yield C_2 via several channels (Welty et al. 2013, and reference therein). C_3 is formed via a dissociative recombination reaction of C_3H^+ , though neutral-neutral reactions (e.g., $C + C_2H_2$) may also contribute to the formation of C_3 (Roueff et al. 2002).

2.2.2 Hydrocarbons - C_nH

The C_nH group represents the simplest hydrocarbons and carbon-chain radicals. All carbon chains from this group have permanent dipole moments and show strong rotational transitions. To date, seven neutral ($n = 2 - 8$) carbon-chain species have been detected from this group. All of them have been identified towards both TMC-1 and IRC+10216. Apart from neutrals, four anions (C_4H^- , C_6H^- , C_8H^- , and $C_{10}H^-$) and two cations (C_3H^+ and C_5H^+) have also been identified in TMC-1. The anions belong to the even series ($n = 2, 4, 6$), while the cations belong to the odd series ($n = 3, 5$). In addition, two cyclic chains, $c-C_3H$, and $c-C_5H$, have been identified. All neutral species have a doublet ground state and show a trend of increasing dipole moment with the number of carbon atoms (n), especially for neutrals and anions (see table 1). The C_nH family is mainly formed through the atomic reactions in the following channel, $C + C_{n-1}H_2 \rightarrow C_nH + H$ (Remijan et al. 2023). Another two channels, which involve atomic and their related anions, can also form C_nH family species efficiently: $C + C_{n-1}H^- \rightarrow C_nH + e^-$ and $H + C_n^- \rightarrow C_nH + e^-$.

2.2.3 Oxygen-bearing carbon chains - C_nO

To date, three oxygen (O)-bearing carbon chains, C_nO ($n = 2, 3, 5$) have been detected in the ISM. In this series, C_3O was the first, detected toward TMC-1 in 1984, while C_2O was identified in the same source in 1991. It took around three decades to detect the higher-order chain, C_5O , in TMC-1. C_4O is yet to be detected. Carbon chains in this group have alternate ground states, i.e., triplet and singlet, and show a trend of increasing dipole moment with the number of carbon

Table 1 (cont'd)

Species	Ground State	Polarizability (α in \AA^3)	Dipole moment (Debye)	Detection Status		
				ISM	TMC-1	IRC+10216
C ₄ Si	singlet	–	6.3 ^w	✓		✓
cyclic-carbon-chains						
<i>c</i> -C ₃ H ₂	singlet	4.58 ^a	3.41 ^a	✓	✓	✓
<i>l</i> -C ₃ H ₂	singlet	5.61 ^a	4.16 ^a	✓	✓	✓
<i>l</i> -C ₅ H ₂	singlet	11.32 ^a	5.89 ^a	✓	✓	
<i>c</i> -C ₃ HCCH	singlet	–	4.93 ^x	✓	✓	
<i>c</i> -H ₂ C ₃ O	singlet	5.20 ^s	4.39 ^s	✓	✓	
PAHs and benzene ring related species						
C ₆ H ₆	singlet	10.35 ^a	0.0	✓		
C ₆₀ ⁺	doublet		0.0	✓		
C ₆₀	singlet	79.0 ^y	0.0	✓		
C ₇₀	singlet	10 ^z	0.0	✓		
<i>c</i> -C ₆ H ₅ CN	singlet	11.91 ^y	4.51 ^{k1}	✓	✓	
<i>c</i> -C ₉ H ₈	singlet	121.20 ^{a1}	0.87 ^{b1}	✓	✓	
<i>c</i> -C ₅ H ₄ CCH ₂	singlet	–	0.69 ^{c1}	✓	✓	
<i>c</i> -C ₅ H ₆	singlet	–	0.42 ^{d1}	✓	✓	
1- <i>c</i> -C ₅ H ₅ CN	singlet	10.93 [*]	4.42 ^{e1}	✓	✓	
2- <i>c</i> -C ₅ H ₅ CN	singlet	10.65 [*]	5.13 ^{e1}	✓	✓	
1-C ₁₀ H ₇ CN	singlet	19.83 [*]	6.6 ^{f1}	✓	✓	
2-C ₁₀ H ₇ CN	singlet	20.43 [*]	6.1 ^{f1}	✓	✓	
1- <i>c</i> -C ₅ H ₅ CCH	singlet	12.36 [*]	1.13 ^{g1}	✓	✓	
2- <i>c</i> -C ₅ H ₅ CCH	singlet	11.93 [*]	1.48 ^{g1}	✓	✓	
<i>o</i> -C ₆ H ₄	singlet	–	1.38 ^{h1}	✓	✓	
C ₆ H ₅ CCH	singlet	–	0.66 ⁱ¹	✓	✓	
C ₉ H ₇ CN	singlet	–	5.04 ^{j1}	✓	✓	

Note. — The ✓ mark in the last three rows means detection including tentative detection.

References: ^aWoon & Herbst (2009), ^bPety et al. (2012), ^cOyama et al. (2020), ^dBlanksby et al. (2001), ^eBotschwina (1991), ^fCrawford et al. (1999), ^gNguyen et al. (2001), ^hBrown et al. (1983), ⁱCernicharo et al. (2020b), ^jEwing (1989), ^kBotschwina (1993), ^lEtim et al. (2020), ^mPascoli & Lavendy (1998), ⁿThaddeus et al. (2008), ^oCernicharo et al. (2008), ^pKawaguchi et al. (1992), ^qHirano et al. (1989), ^rBotschwina (1987), ^sKIDA (<https://kida.astrochem-tools.org/>), ^tWoon (1996), ^uCernicharo et al. (2019), ^vPardo et al. (2022), ^wOhishi et al. (1989), ^xTravers et al. (1997), ^y<https://cccbdb.nist.gov/pollstx.asp>, ^zCompagnon et al. (2001), ^{a1}Ghiasi & Monnajemi (2006), ^{b1}Caminati (1993), ^{c1}Sakaizumi et al. (1993a), ^{d1}Laurie (1956), ^{e1}Sakaizumi et al. (1987), ^{f1}McNaughton et al. (2018), ^{g1}(Cernicharo et al. 2021d), ^{h1}Kraka & Cremer (1993), ⁱ¹Cox et al. (1975), ^{j1}Sita et al. (2022), ^{k1}Wohlfart et al. (2008), ^{l1}Puzzarini (2008), ^{m1}Mohamed et al. (2005), ⁿ¹Marcelino et al. (2020), ^{o1}Cabezas et al. (2022a), ^{p1}Fuentetaja et al. (2022a), ^{q1}Gordon et al. (2002), ^{r1}Wang et al. (2009) *This work (estimated with B3LYP/6-311++G(d,p) level of theory using Gaussian software (Frisch et al. 2013))

atoms (see table 1). A protonated species, HC_3O^+ with singlet ground state, has been detected in TMC-1 (Cernicharo et al. 2020b). The observed trend toward TMC-1 shows that C_3O is the most abundant, followed by C_2O and C_5O , with C_5O about 50 times less abundant than C_2O and about 80 times less abundant than C_3O (Cernicharo et al. 2021a). In addition, all these species have been identified towards the circumstellar envelope of IRC+10216. The formation of C_nO and HC_nO chains follows similar formation mechanisms as discussed above. The first step involves the radiative association of C_{n-1}H^+ , $\text{C}_{n-1}\text{H}_2^+$, and $\text{C}_{n-1}\text{H}_3^+$ ions with CO, which is then followed by dissociative electron recombination reactions (Adams et al. 1989; Cernicharo et al. 2021a).

2.2.4 Sulfur-bearing carbon chains - C_nS

Similar to C_nO , several sulfur (S)-bearing carbon chains, C_nS ($n = 2, 3, 4, 5$), have been identified in the ISM. Two protonated species, HCCS^+ and HC_3S^+ , have only been detected towards TMC-1 so far. Carbon chains in this group have alternative ground states, i.e., triplet and singlet, and show a trend of increasing dipole moment with the number of carbon atoms, similar to the C_nO group (see table 1). The abundances of C_2S and C_3S are almost three orders of magnitude higher than C_4S and C_5S toward TMC-1 (Cernicharo et al. 2021f). On the other hand, the C_5S column density is slightly less than those of C_2S and C_3S , with differences less than one order of magnitude, toward IRC+10216 (Agúndez et al. 2014). C_2S and C_3S are mainly produced via several ion-neutral reactions followed by electron recombination reactions and via several neutral-neutral reactions (Sakai et al. 2007). Higher order chains of this family, such as C_4S and C_5S , are thought to be formed via reactions of $\text{S} + \text{C}_4\text{H}$ and $\text{C} + \text{HC}_3\text{S}$, and $\text{C}_4\text{H} + \text{CS}$ and $\text{S} + \text{C}_5\text{H}$, respectively. However, the kinetics and product distribution of these reactions are poorly known (Cernicharo et al. 2021f).

2.2.5 Nitrogen-bearing carbon chains - C_nN

In this group, C_3N was the first detected species, done so tentatively toward IRC+10216 in 1977 and more robustly toward TMC-1 in 1980. The next higher order chain in this series, C_5N was detected toward TMC-1 and tentatively detected toward IRC+10216 in 1998. The lower order chain, CCN , was found in 2014. Their anions, C_3N^- and C_5N^- , were discovered in the circumstellar envelope of the carbon-rich star IRC+10216 (Thaddeus et al. 2008; Cernicharo et al. 2008). They have also been identified toward TMC-1 by the QUIJOTE group, including their neutral analogs (C_3N , C_5N) (Cernicharo et al. 2020c). They measured similar abundance ratios of $\text{C}_3\text{N}^-/\text{C}_3\text{N} = 140$ and 194 , and $\text{C}_5\text{N}^-/\text{C}_5\text{N} = 2$ and 2.3 in TMC-1 and IRC+10216, re-

spectively, even though physical conditions are completely different for TMC-1 and IRC+10216. It might be a coincidence that there are similar abundance ratios of anion and neutral forms of C_nN ($n = 3, 5$). All carbon chains from this group have doublet ground state, and the two anionic forms have singlet state. Since the dipole moment of CCN is low compared to those of C_3N , C_5N , and their anionic forms, the detection of CCN is more challenging, even though it is of lower order in the chain (see table 1). C_4N , C_6N , and C_7N show even smaller values of their dipole moments, which suggests that much high sensitivity observations are required for their identification. C_2N is produced through the reactions of $N + C_2$ and $C + CN$. Similarly, C_3N is produced in reactions of $N + C_3$ and $C + CCN$, and C_5N is produced through $N + C_5$ on dust surfaces⁴. The production of C_3N^- mainly comes from the reaction between N atoms and bare carbon-chain anions C_n^- (Cernicharo et al. 2020c), whereas C_5N^- is produced via the electron radiative attachment to C_5N (Walsh et al. 2009).

2.2.6 Phosphorus-bearing carbon chains - C_nP

Although phosphorus (P) has a relatively small elemental abundance, it plays a crucial role in the development of life (Chantzios et al. 2020). Among the known eight phosphorus-bearing molecules, C_2P (or CCP) is the only P-bearing carbon-chain species and detected toward IRC+10216 (Halfen et al. 2008). All carbon chains in this group have doublet ground states (table 1). Higher order chains, C_3P and C_4P , show a higher value of dipole moments, but they are yet to be detected in the ISM or circumstellar environments. Since the overall elemental abundance of phosphorous is small, higher-order phosphorous chains are expected to have very low abundances. CCP may be produced by radical-radical reactions, between CP and hydrocarbons (CCH and C_3H), or ion-molecule chemistry involving P^+ and HCCH followed by the dissociative electron recombination reaction (Halfen et al. 2008).

2.2.7 HC_nO family

Four neutral HC_nO ($n = 2, 3, 5, 7$) chains have been identified toward TMC-1 (Cernicharo et al. 2021a; McGuire et al. 2017; Cordiner et al. 2017). The detection summary of this group indicates odd n chains are more abundant compared to their even n counterparts. This trend is the same as in the C_nO family. All neutral chains have doublet ground states and dipole moment values are less than 3 Debye. The observed cation HC_3O^+ has a singlet ground state and a dipole moment of 3.41 Debye (see table 1). As mentioned before, C_nO and HC_nO are linked through their formation routes (see Sec. 2.2.3).

⁴<https://kida.astrochem-tools.org/>

2.2.8 HC_nS family

This family is similar to HC_nO but contains sulfur instead of oxygen. Only two neutral species, HCCS and HC₄S have been identified toward TMC-1 (Cernicharo et al. 2021f; Fuentetaja et al. 2022a). Observed statistics suggest chains with even n have higher abundance than odd n species. All neutral chains of this group have doublet ground states (see table 1). The dipole moments of neutral species are less than 2.2 Debye. HCCS is mainly formed through the reaction, C + H₂CS (Cernicharo et al. 2021f). HC₄S is produced through the reaction between C and H₂C₃S and by the dissociative recombination reaction of H₂C₄S⁺, which is formed via reactions of S + C₄H₃⁺ and S⁺ + C₄H₃ (Fuentetaja et al. 2022b). This group has protonated ions, and HC₂S⁺ and HC₃S⁺ have been detected in TMC-1 (Cabezas et al. 2022b; Cernicharo et al. 2021e). For HC₃S⁺, proton transfer to C₃S from HCO⁺ and H₃O⁺ is the main formation route. The reactions of S⁺ + $c, l - C_3H_2$ and S + $c, l - C_3H_3$ are also equally important and efficient (Cernicharo et al. 2021e).

2.2.9 Cyanopolyynes - HC_{2n+1}N

Cyanopolyynes are the most important, interesting, and ubiquitous organic carbon chains ($n = 1 - 5$) detected in the ISM so far. As mentioned above, HC₃N was the first detected carbon-chain molecule in space. In this series, five species, starting from HC₃N to HC₁₁N, have been found in TMC-1. All these species have also been detected toward IRC+10216, except HC₁₁N (Morris et al. 1976; Winnewisser & Walmsley 1978; Matthews et al. 1985). In this series, especially HC₃N and HC₅N, have been identified in various star-forming environments (see section 3.3.2). Three cations, HC₃NH⁺, HC₅NH⁺, and HC₇NH⁺, have also been identified toward TMC-1 (Kawaguchi et al. 1994; Marcelino et al. 2020; Cabezas et al. 2022a). All neutral cyanopolyynes have a singlet ground state and show a trend of increasing dipole moment with length of the chain (see table 1). Unlike other carbon-chain species, the cyanopolyyne family could form on dust surfaces through reactions N + C_{2n+1}H ($n = 1 - 4$) and H + C_{2n+1}N ($n = 1 - 4$) (see section 3.1.2 for more detail regarding the formation of cyanopolyynes in the gas phase). Protonated cyanopolyynes (e.g., HC₃NH⁺, HC₅NH⁺) are mainly formed via a proton donor (e.g., HCO⁺) to cyanopolyynes (e.g., HC₃N, HC₅N). Protonated cyanopolyynes are destroyed by dissociative electron recombination reactions (Marcelino et al. 2020).

2.2.10 Allenic chain family - HC_{2n}N

HCCN was the first member of the allenic chain family, HC_{2n}N, observed in space (Guelin & Cernicharo 1991), and HC₄N was the second. These species have been identified toward

IRC+10216. The allenic chain family has a triplet ground state and shows increasing dipole moment with size, similar to cyanopolyynes and other families (table 1). HC_4N may form through the reactions of $\text{C}_3\text{N} + \text{CH}_2$ and $\text{C}_3\text{H} + \text{HCN}$. For this family, ion-molecule paths are relatively slow (Cernicharo et al. 2004). However, HCCN is formed by the reactions between atomic nitrogen and H_nCCH^+ .

2.3 Statistics of Detected Species

About 300 individual molecular species have been identified in the ISM and circumstellar envelopes by astronomical observations to date (CDMS⁵, McGuire (2022)). Most of them are observed in the gas phase via their rotational transition lines, and very few of them are observed in the solid phase. Carbon is the fourth most abundant element in the Galaxy (e.g., Asplund et al. 2009) and plays a pivotal role in interstellar chemistry. A variety of carbon-chain species have been identified in the space ranging from simple linear chains to cyclic and PAHs. In this subsection, we present statistics of the detections that have been reported by the end of 2022.

Figure 2 shows the cumulative plot of carbon-chain detection together with the histogram plot in each year starting from 1971, the first carbon-chain detection year, until 2022. Following the definition mentioned earlier in section 1.3, 118 carbon-chain species have been discovered until the end of 2022. This accounts for approximately 44% of all the known 270 molecules (the total number of identified interstellar molecules at the end of 2022). Following the discovery of HC_3N in 1971 (Turner 1971), new carbon-chain species continued to be found at a rate of just over one species per year for the next 50 years. A steep increase is seen in 2021 and 2022 in figure 2, thanks to the two deep line survey projects toward TMC-1 CP (section 3.1.1).

Figure 3 illustrates the detection statistics of all known carbon-chain species per decade starting from the 1970s. Figure 3 basically summarizes the information of figure 2, but summing up each decade. It shows the detection of carbon-chain species in each decade was similar starting from the 1970s to the 2010s. Around 50 molecular species, which account for 42% of the carbon-chain species detected in the ISM, have been discovered in the last three years (2020-2022), achieved by two sensitive line survey projects toward TMC-1. These survey projects detect many types of carbon-chain species, including large linear and ring hydrocarbons and species including benzene rings. These results are attributed to the development of facilities for radio telescopes and new analytical methods. Thus, there has been a dramatic change

⁵<https://cdms.astro.uni-koeln.de/classic/molecules>

in discovered carbon-chain species in the 2020s. The point to be emphasized here is that in just three years of the current decade enormous progress has been made and discoveries are continuing at a rapid pace. Carbon-chain species that have been detected so far and candidates for future detection are summarized in table 1.

2.4 Warm Carbon-Chain Chemistry (WCCC)

In section 1.2, we mentioned that carbon-chain molecules have been classically known as early-type species, because they are abundant in young starless cores and deficient in evolved star-forming cores. Against this classical picture, Sakai et al. (2008) detected various carbon-chain molecules toward IRAS 04368+2557 in the low-mass star-forming region L1527 in Taurus. The derived rotational temperature from the C_4H_2 lines is 12.3 ± 0.8 K, which is higher than excitation temperatures of carbon-chain species in the starless core TMC-1 ($\approx 4-8$ K). They proposed that evaporation of CH_4 from ice mantles could be the trigger of formation of carbon-chain molecules in the lukewarm envelopes around low-mass protostars, and named such a carbon-chain formation mechanism “Warm Carbon-Chain Chemistry (WCCC)”. A second WCCC source, IRAS 15398-3359 in the Lupus star-forming region, was discovered soon after (Sakai et al. 2009). This suggested that the WCCC mechanism may be a common feature around low-mass protostars, and WCCC has been widely accepted in the astrochemical field.

Later studies using chemical simulations support the formation mechanism of carbon-chain molecules starting from CH_4 around temperatures of 25–30 K (Hassel et al. 2008). The CH_4 molecules react with C^+ in the gas phase to produce $C_2H_3^+$ or $C_2H_2^+$. The $C_2H_2^+$ ion reacts with H_2 leading to $C_2H_4^+$. Then, electron recombination reactions of $C_2H_3^+$ and $C_2H_4^+$ produce C_2H_2 . Regarding WCCC, the review article by Sakai & Yamamoto (2013) summarized related studies in detail. We thus avoid duplication here.

However, an important question has been raised since the review of Sakai & Yamamoto (2013), namely, the origin(s) of WCCC sources, which is still controversial. The focus is on how CH_4 -rich ice is formed. This means that carbon atoms need to be adsorbed onto dust grains without being locked up in CO molecules. Sakai et al. (2008) proposed one possible scenario that shorter collapse times of prestellar cores may produce conditions needed for WCCC sources. On the other hand, Spezzano et al. (2016) suggested that variations in the far ultraviolet (FUV) interstellar radiation field (ISRF) could produce carbon-chain-rich or COM-rich conditions, based on their observational results toward the prestellar core L1544. They found a spatial distribution of *c*- C_3H_2 in a region relatively exposed to the ISRF, while CH_3OH was found

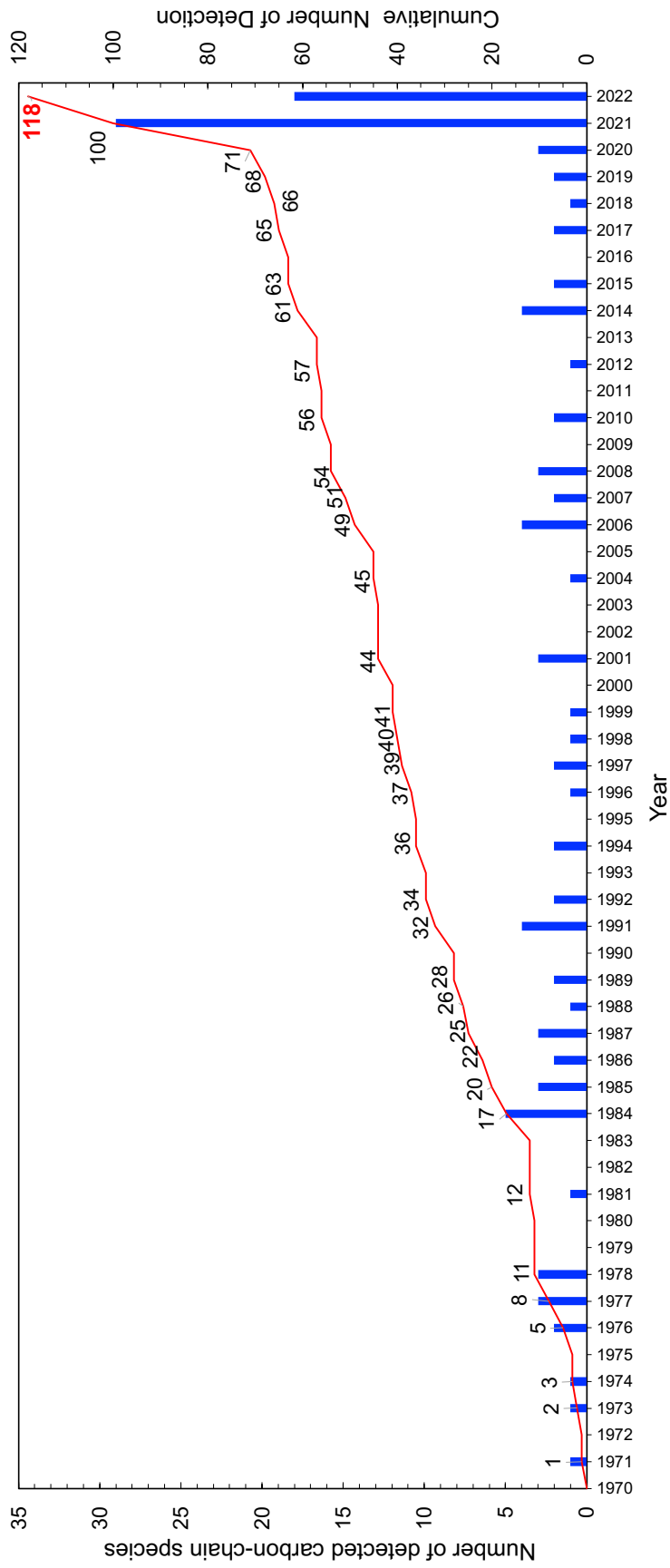


Fig. 2 The number of detected carbon-chain species in each year (blue bars) and its cumulative plot (red curves and numbers).

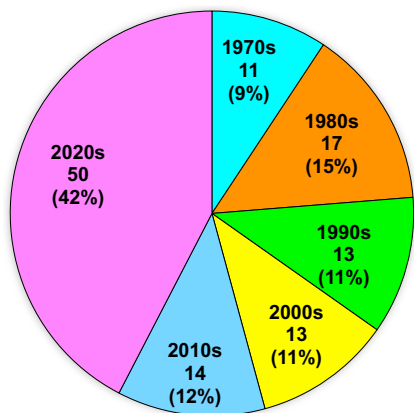


Fig. 3 Proportion of detected carbon-chain species every 10 years and in the three years of the 2020s.

in a relatively shielded region. In this scenario, the FUV ISRF destroys CO, a precursor of CH₃OH, leading to formation of C and/or C⁺, precursors of carbon-chain species. Spezzano et al. (2020) also found similar trends with observations of *c*-C₃H₂ and CH₃OH toward six starless cores. They concluded that the large-scale effects have a direct impact on the chemical segregation; *c*-C₃H₂ is enhanced in the region more illuminated by the ISRF, whereas CH₃OH tends to reside in the region shielded from the ISRF. Such chemical segregation observed in starless cores may be inherited to the protostellar stage and recognized as the different classes of WCCC protostars and COM-rich hot corinos. Recently, several authors investigated the effects of these factors on the abundances of carbon-chain species and COMs by chemical simulations (Aikawa et al. 2020; Kalvāns 2021). We discuss their model results in detail in section 4.

2.5 Concept of Hot Carbon-Chain Chemistry

The discovery of the WCCC mechanism around low-mass protostars naturally raised a question: are carbon-chain molecules also formed around high-mass ($m_* > 8M_\odot$) protostars? With such a motivation, observations and chemical simulations focusing on carbon-chain species around massive young stellar objects (MYSOs) have proceeded since the late 2010s. Observational studies show that carbon-chain species are abundant around some MYSOs, but their abundances, especially cyanopolyynes, cannot be reproduced by WCCC. Then, a different carbon-chain chemistry has been proposed (Taniguchi et al. 2023). Here, we briefly explain the concept of “Hot Carbon-Chain Chemistry (HCCC)” proposed to reproduce the observational results around MYSOs. Details of these observational and simulation studies are summarized in sections 3.3 and 4, respectively.

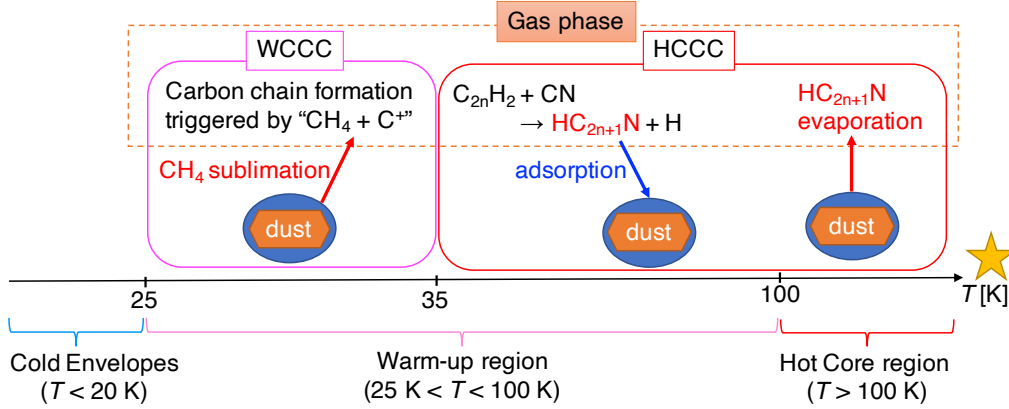


Fig. 4 Temperature dependence of carbon-chain chemistry. WCCC occurs around 25–35 K, while HCCC occurs in higher-temperature regions.

Figure 4 shows a schematic view of carbon-chain chemistry around MYSOs based on the result of the chemical simulation by Taniguchi et al. (2019a). We distinguish HCCC from WCCC depending on the temperature. The HCCC mechanism refers to carbon-chain formation in the gas phase, adsorption onto dust grains, and accumulation in ice mantles during the warm-up phase ($25 \text{ K} < T < 100 \text{ K}$), followed by evaporation into the gas phase in the hot-core stage ($T > 100 \text{ K}$).

This mechanism is particularly important for cyanopolyynes (HC_{2n+1}N). Cyanopolyynes are relatively stable species because of no dangling bond, and they are not destroyed in the gas phase by reactions with O or H_2 , which are major destroyers of other carbon-chain species with dangling bonds. Instead, cyanopolyynes are consumed by reactions with protonated ions such as HCO^+ in the gas phase. Thus, the gas-phase destruction rates of cyanopolyynes are lower than those of the other carbon-chain species, which enables cyanopolyynes to be adsorbed onto dust grains. During the warm-up stage, cyanopolyynes are efficiently formed by the gas-phase reactions between C_{2n}H_2 and CN. The formed cyanopolyynes are then adsorbed onto dust grains and accumulated in ice mantles. When conditions reach their sublimation temperatures above 100 K, the species sublime into the gas phase and their gas-phase abundances show peaks.

Radical-type species, such as CCH and CCS, would not behave as cyanopolyynes do, because they are efficiently destroyed by the gas-phase reactions with O or H_2 (Taniguchi et al. 2019a). Their gas-phase peak abundances are reached just after WCCC starts to form them around 25 K, and decrease as the temperature increases. Thus, we expect that radical-type

carbon-chain species are abundant in the lukewarm regions and deficient in the hot-core regions, whereas the emission of cyanopolyynes is expected to show their peaks at the hot-core regions, similar to the emission of COMs.

The points of this section are summarized below.

1. Carbon-chain molecules account for around 40% of the interstellar molecules. These molecules have been detected in the ISM since the 1970s, and an increased number of reported detections made by recent Green Bank 100m telescope (GBT) and Yebes 40m telescope observations are astonishing.
2. WCCC refers to the carbon-chain formation mechanism in the lukewarm gas ($T \approx 25 - 35$ K) starting from CH_4 desorbing from dust grains around 25 K. The gas-phase reaction between CH_4 and C^+ is the trigger of the WCCC mechanism.
3. HCCC refers to the gas-phase carbon-chain formation and adsorption and accumulation in ice mantles during the warm-up phase ($T < 100$ K), and their sublimation in the hot-core phase ($T > 100$ K).

3 Observations

3.1 Carbon-Chain Species in Dark Clouds

3.1.1 Carbon-Chain Molecules in TMC-1

Taurus Molecular Cloud-1 (TMC-1) is one of the most well-studied filament (e.g., Kaifu et al. 2004). Its ‘‘Cyanopolyne Peak’’ (hereafter TMC-1 CP) is the famous site where carbon-chain molecules are particularly abundant (figure 5). Many carbon-chain molecules were discovered from this dark cloud by radio astronomical observations (section 2.1).

Dobashi et al. (2018) identified four velocity components ($v_{\text{LSR}} = 5.727, 5.901, 6.064,$ and 6.160 km s^{-1}) at TMC-1 CP with very high velocity resolution (0.0004 km s^{-1}) spectra of the CCS and HC_3N lines in the 45 GHz band obtained by the Z45 receiver (Nakamura et al. 2015) installed on the Nobeyama 45m radio telescope. They revealed the gas kinematics of the TMC-1 filament and found that these four velocity components indicate moving inward toward the center of the TMC-1 filament. Dobashi et al. (2019) identified 21 subfilaments in the TMC-1 filament using CCS ($J_N = 4_3 - 3_2$; 45.379033 GHz) line data. They found that the subfilaments have line densities that are close to the critical line density for dynamical equilibrium ($\sim 17M_\odot \text{ pc}^{-1}$). These results indicate that self-gravity is important in the dynamics of the subfilaments. The CCS ($J_N = 4_3 - 3_2$) line was also used for measurement of the line-of-sight magnetic field strength by its Zeeman splitting (Nakamura et al. 2019). The derived

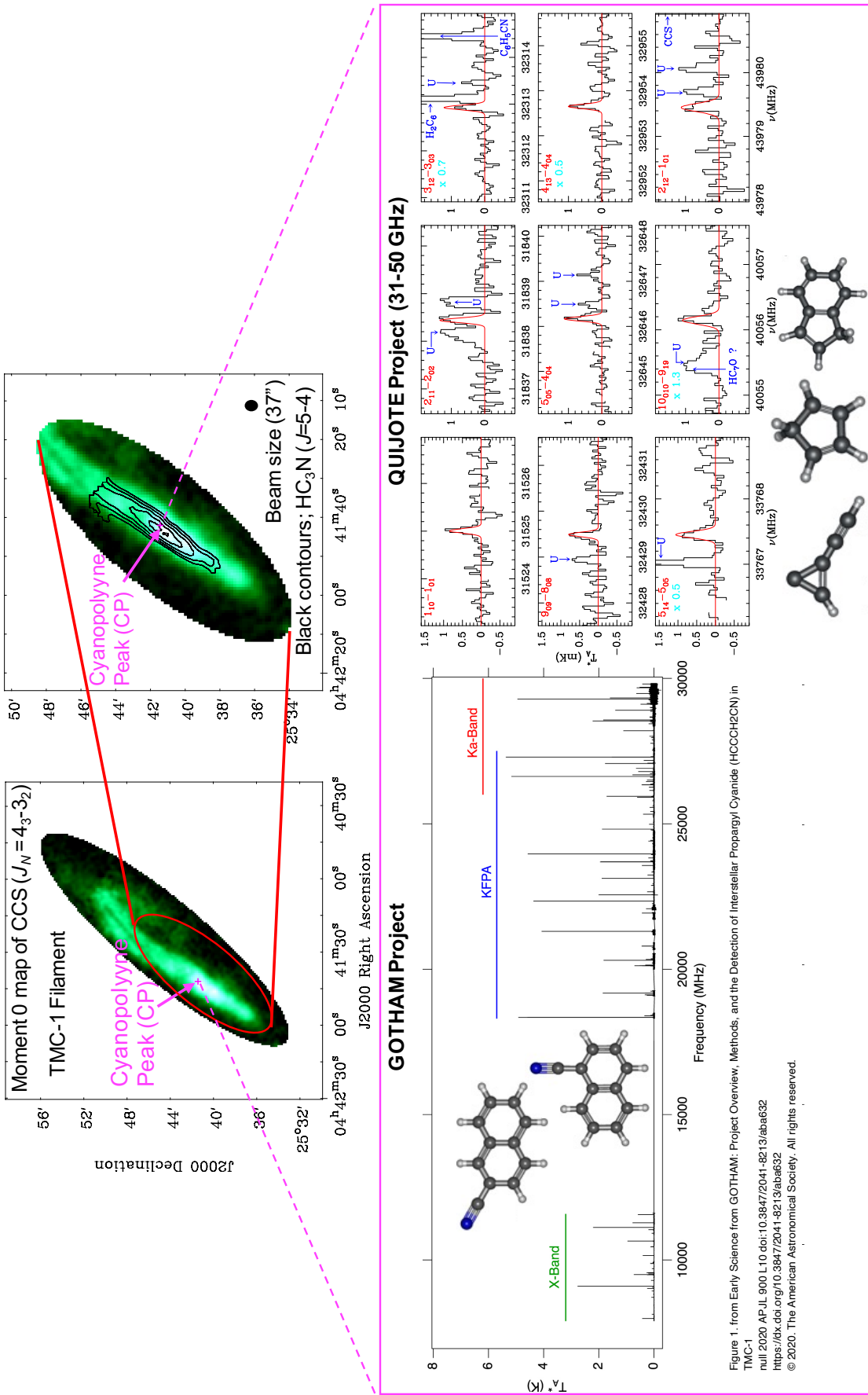


Fig. 5 Top panels: Moment 0 map of the CCS ($J_N = 4_3 - 3_2$) line overlaid by black contours indicating moment 0 map of the HC_3N ($J = 5 - 4$) line. These data were obtained with the Nobeyama 45m radio telescope (beam size= $37''$ at 45 GHz). The original data were provided by Dr. Fumitaka Nakamura (NAOJ) and Dr. Kazuhito Dobashi (Tokyo Gakugei University). The magenta cross shows the position of the Cyanopolyyne Peak (TMC-1 CP) observed by the two line survey projects, GOTHAM and QUIJOTE projects. The spectral figures are from McGuire et al. (2020) and Cernicharo et al. (2021b).

magnetic field strength is $\sim 117 \pm 21 \mu\text{G}$, which implies that the TMC-1 filament is magnetically supercritical. As these studies show, rotational-transition lines of carbon-chain species are useful to investigate physical conditions of starless cores.

Two research groups have been carrying out line survey observations toward TMC-1 CP and have reported the detection of new interstellar molecules. Their researches are still ongoing as of the writing of this review article. Here we highlight groundbreaking results done by each project.

One project is GOTHAM (GBT Observations of TMC-1: Hunting Aromatic Molecules⁶) using the Green Bank 100m telescope. This project is a high sensitivity (2 mK) and high velocity resolution (0.02 km s^{-1}) spectral line survey in the X, K, and Ka bands (see Fig. 5). The beam sizes (FWHM) are $1.4'$, $32''$, and $26.8''$ for the X-Band receiver, KFPA, and Ka-Band (MM-F1) receiver, respectively⁷. They have analyzed spectra using the spectral line stacking and matched filter methods (Loomis et al. 2018b, 2021) utilizing the velocity information derived by Dobashi et al. (2018), and achieved detection of new, rare interstellar molecules.

McGuire et al. (2021) detected two polycyclic aromatic hydrocarbons (PAHs), 1- and 2-cyanonaphthalene, containing two rings of benzene via spectral matched filtering. Some strong lines of 1-cyanonaphthalene can be identified in the smoothed spectra with a 14-kHz resolution. Their molecular structures are shown in figure 5. The nitrile bond (-CN) makes the dipole moment larger, thus aiding the detection of benzonitrile ($c\text{-C}_6\text{H}_5\text{CN}$), the first detected species with a benzene ring at TMC-1 CP (McGuire et al. 2018). Benzonitrile has also been detected in other sources: Serpens 1A, Serpens 1B, Serpens 2, and L1521F (Burkhardt et al. 2021a). Although the detection of pure hydrocarbon rings was considered to be difficult due to their small permanent dipole moments, Burkhardt et al. (2021b) achieved the detection of indene ($c\text{-C}_9\text{H}_8$). McCarthy et al. (2021) detected 1-cyano-1,3-cyclopentadiene ($c\text{-C}_5\text{H}_5\text{CN}$), a five-membered ring, and Lee et al. (2021) detected 2-cyano-1,3-cyclopentadiene, which is an isomer with a little higher energy (5 kJ mol^{-1} or 600 K). Thus, not only molecules with benzene structure, but also molecules with five-membered rings with a nitrile bond have been detected. Loomis et al. (2021) reported the detection of HC_{11}N . HC_4NC , an isomer of HC_5N , has been detected by Xue et al. (2020), and soon after Cernicharo et al. (2020a) also reported its detection using the Yebes 40m telescope. Xue et al. (2020) ran chemical simulations with formation pathways of electron recombination reactions of HC_5NH^+ and HC_4NCH^+ , and reproduced the observed abundance of HC_4NC .

⁶ <https://greenbankobservatory.org/science/gbt-surveys/gotham-survey/>

⁷ <https://www.gb.nrao.edu/scienceDocs/GBTpg.pdf>

The other project is QUIJOTE (Q-band Ultrasensitive Inspection Journey to the Obscure TMC-1 Environment) line survey using the Yebes 40m telescope. This line survey project covers 31.0–50.3 GHz with a frequency resolution of 38.15 kHz, corresponding to ~ 0.29 km s⁻¹ at 40 GHz. They have achieved sensitivities of 0.1 – 0.3 mK and various molecules have been successfully detected without stacking analyses. The beam sizes are 56'' and 31'' at 31 GHz and 50 GHz, respectively (Fuentetaja et al. 2022a).

This group reported the detection of many pure hydrocarbons consisting of only carbon and hydrogen: e.g., 1- and 2-ethynyl-1,3-cyclopentadiene (*c*-C₅H₅CCH, Cernicharo et al. 2021d); benzyne (*ortho*-C₆H₄, Cernicharo et al. 2021c); *c*-C₃HCCH, *c*-C₅H₆, *c*-C₉H₈ (Cernicharo et al. 2021b); fulvenallene (*c*-C₅H₄CCH₂, Cernicharo et al. 2022c); and CH₂CCHC₄H (Fuentetaja et al. 2022b). The detection of such pure hydrocarbons is astonishing because their dipole moments are very small. In addition to pure hydrocarbons, the QUIJOTE project has also detected carbon-chain ions: e.g., HC₃O⁺ (Cernicharo et al. 2020b); HC₇NH⁺ (Cabezas et al. 2022a); HC₃S⁺ (Cernicharo et al. 2021e); HCCS⁺ (Cabezas et al. 2022b); C₅H⁺ (Cernicharo et al. 2022b). It has also detected five cyano derivatives (*trans*-CH₃CHCHCN, *cis*-CH₃CHCHCN, CH₂C(CH₃)CN, *gauche*-CH₂CHCH₂CN, *cis*-CH₂CHCH₂CN; Cernicharo et al. 2022a). The very high sensitivity line survey observations achieved by the QUIJOTE project reveal a wide variety of carbon-chain species. At the same time, these results raise new questions because the abundances of some of the newly detected molecules cannot be explained by chemical models.

3.1.2 Revealing Main Formation Pathways of Carbon-Chain Molecules by ¹³C Isotopic Fractionation

Since carbon-chain molecules are unstable even in vacuum chambers on the Earth, it is difficult to conduct laboratory experiments about their reactivity. Then, their formation and destruction reactions remain unclear. Instead, the observed ¹³C isotopic fractionation of carbon-chain molecules, which refers to the relative differences in abundance among the ¹³C isotopologues, was proposed to be a key method for revealing their main formation mechanisms (Takano et al. 1998). The ¹³C isotopic fractionation is effective only in low-temperature conditions as it depends mainly on isotope exchange reactions, whose backward reactions can proceed only at warm or high temperatures. The elemental ¹²C/¹³C abundance ratio in the local ISM is around 60–70 (e.g., Milam et al. 2005). Hence, high-sensitivity observations are necessary to detect the ¹³C isotopologues of carbon-chain molecules with high enough signal-to-noise (S/N) ratios to compare their abundances. With these constraints, TMC-1 CP is the most promising target source, because of the low-temperature condition ($T \approx 10$ K) and high abundances of

Table 2 Main formation mechanisms of HC₃N and expected ¹³C isotopic fractionation

Formation Route	Expected fractionation pattern	Starless cores
C ₂ H ₂ + CN → HC ₃ N + H	1 : 1 : <i>x</i>	TMC-1 CP, L1521B
CCH + HNC → HC ₃ N + H	<i>y</i> : 1 : <i>z</i>	L134N
HC ₃ NH ⁺ + e ⁻ → HC ₃ N + H	≈ 1 : 1 : 1	...

“Expected fractionation pattern” means the [H¹³CCCN]:[HC¹³CCN]:[HCC¹³CN] ratio. Here *x*, *y*, and *z* are arbitrary values.

carbon-chain molecules (section 3.1.1). In fact, TMC-1 CP has the largest number of carbon-chain species investigated for ¹³C isotopic fractionation: seven species have been studied, HC₃N (Takano et al. 1998), CCS (Sakai et al. 2007), CCH (Sakai et al. 2010), C₃S and C₄H (Sakai et al. 2013), HC₅N (Taniguchi et al. 2016a), HC₇N (Burkhardt et al. 2018). Thanks to advent of new observational facilities, larger molecules can be investigated within reasonable observing times. The same method has also been applied to other molecular clouds and envelopes around YSOs. In this subsection, we review such studies conducted in dark clouds.

Three cyanopolyynes have been investigated at TMC-1 CP; HC₃N (Takano et al. 1998), HC₅N (Taniguchi et al. 2016a), and HC₇N (Burkhardt et al. 2018). Takano et al. (1998) observed the three ¹³C isotopologues of HC₃N (H¹³CCCN, HC¹³CCN, and HCC¹³CN) using the Nobeyama 45m radio telescope. The relative abundance ratios of the three ¹³C isotopologues were derived to be 1.0 : 1.0 : 1.4 (±0.2) (1σ) for [H¹³CCCN]:[HC¹³CCN]:[HCC¹³CN]. Table 2 summarizes correspondences of the possible main formation pathway of HC₃N and its expected ¹³C isotopic fractionation (Taniguchi et al. 2017a). Regarding the last one (the electron recombination reaction of HC₃NH⁺), various formation pathways of the HC₃NH⁺ ion should compete, and then clear ¹³C isotopic fractionation would not be seen in HC₃NH⁺, as well as HC₃N. The reaction between of “C₂H₂ + CN → HC₃N + H” can explain the observed ¹³C isotopic fractionation in TMC-1 CP.

At the time five ¹³C isotopologues of HC₅N were detected (Takano et al. 1990) there was no evidence for the ¹³C isotopic fractionation, because S/N ratios were low. More than 25 years later, Taniguchi et al. (2016a) successfully detected the lines of the five ¹³C isotopologues of HC₅N (*J* = 9 – 8 and 16 – 15 at 23 GHz and 42 GHz bands, respectively) with sufficient S/N ratios of 12–20. The derived abundance ratios among the five ¹³C isotopologues of HC₅N are 1.00 : 0.97 : 1.03 : 1.05 : 1.16 (±0.19) (1σ) for [H¹³CCCCCN] : [HC¹³CCCCN] : [HCC¹³CCCN] : [HCCC¹³CCN] : [HCCCC¹³CN]. Hence, even if the S/N ratios increase, there is no clear difference in abundance among the five ¹³C isotopologues of HC₅N, unlike HC₃N. Taniguchi

et al. (2016a) proposed that the reactions between hydrocarbon ions ($C_5H_m^+$; $m = 3 - 5$) and nitrogen atoms, followed by electron recombination reactions are the most plausible main formation mechanism of HC_5N at TMC-1 CP.

Burkhardt et al. (2018) detected six ^{13}C isotopologues of HC_7N and five ^{13}C isotopomers of HC_5N using the Green Bank 100m telescope. $H^{13}CC_6N$ could not be detected in their observations. They found no significant difference among the ^{13}C isotopomers of HC_7N , as similar to the case of HC_5N . They concluded that the significant formation route for HC_7N is the reaction of hydrocarbon ions and nitrogen atoms, which is the same conclusion for HC_5N by Taniguchi et al. (2016a).

HC_3N has been investigated in two other starless cores, L1521B and L134N (L183) (Taniguchi et al. 2017a). Their observational results show different fractionation patterns between the two sources. The ^{13}C isotopic fractionation in L1521B is similar to that in TMC-1 CP; $HCC^{13}CN$ is more abundant than the others, and the other two ^{13}C isotopologues have similar abundances. On the other hand, the results in L134N are different from TMC-1 CP and L1521B; the abundance ratios in L134N are $1.5 (\pm 0.2) : 1.0 : 2.1 (\pm 0.4)$ (1σ) for $[H^{13}CCCN]:[HC^{13}CCN]:[HCC^{13}CN]$. The last column of table 2 summarizes the names of molecular clouds that were suggested to have each main formation route. Based on these classifications (table 2), the main formation mechanisms of HC_3N are determined as the reactions of $C_2H_2 + CN$ in L1521B and $CCH + HNC$ in L134N. The $C^{13}CH/^{13}CCH$ abundance ratio was found to be > 1.4 in L134N (Taniguchi et al. 2019b), which agrees with the abundance ratio of $1.5 (\pm 0.2) : 1.0$ for $[H^{13}CCCN]:[HC^{13}CCN]$. This is further supporting evidence for the conclusion that the main formation pathway of HC_3N includes CCH in L134N. The difference between L134N and TMC-1CP/L1521B is probably brought about by different HNC/CN abundance ratios (HNC/CN = 35.6 and 54.2 in TMC-1 CP and L134N, respectively). The HNC/CN abundance ratio depends on the cloud age, and then the main formation mechanism of cyanopolyynes likely changes over the course of the cloud evolution.

In addition to cyanopolyynes, C_nS ($n = 2, 3$) and $C_{2n}H$ ($n = 1, 2$) have been studied for ^{13}C fractionation in TMC-1 CP (Sakai et al. 2007, 2010, 2013). Sakai et al. (2007) detected the lines of ^{13}CCS and $C^{13}CS$ ($J_N = 2_1 - 1_0$, $F = 5/2 - 3/2$). The abundance ratio of $C^{13}CS/^{13}CCS$ was derived to be 4.2 ± 2.3 (3σ). They proposed that the reaction between CH and CS is the main formation route of CCS in TMC-1 CP. The abundance ratio of $C^{13}CH/^{13}CCH$ was derived to be 1.6 ± 0.4 (3σ) (Sakai et al. 2010). To explain the abundance difference between the two ^{13}C isotopomers of CCH, Sakai et al. (2010) proposed that the reaction of $CH + C$ is the main formation mechanism of CCH at TMC-1 CP.

Unlike cyanopolyynes, the ^{13}C isotopic fractionation of CCS and CCH does not necessarily provide information on their main formation mechanisms. Furuya et al. (2011) ran chemical simulations including ^{13}C and investigated effects of the isotopomer-exchange reactions. They considered the following two isotopomer-exchange reactions for CCH and CCS, respectively:



and



They also included the following neutral-neutral exchange reaction of CCS to reproduce the observed isotopomer ratio of CCS:



This reaction is regarded as a catalytic reaction by the hydrogen atom. At low temperature conditions ($T \approx 10$ K), C^{13}CH and C^{13}CS should be more abundant than the other ^{13}C isotopomers by Reactions (1) – (3). Their model results can explain the observed abundance differences between the two ^{13}C isotopomers of CCH and CCS in TMC-1 CP (Sakai et al. 2007, 2010). It was found that C^{13}CH is more abundant than ^{13}CCH in the other starless cores (L1521B and L134N; Taniguchi et al. 2019b), and such a character may be common for cold dark clouds. Such exchange reactions may contribute to larger species such as C_3S and C_4H (Sakai et al. 2013).

3.1.3 Dilution of the ^{13}C species

From the observations deriving the ^{13}C isotopic fractionation of carbon-chain species in dark clouds, dilution of the ^{13}C species is inferred, i.e., the $^{12}\text{C}/^{13}\text{C}$ ratios of carbon-chain molecules are higher than the local elemental abundance ratio (60–70; Milam et al. 2005). The variations of the $^{12}\text{C}/^{13}\text{C}$ ratios of carbon-chain species could give another hint about carbon-chain chemistry in dark clouds. This is caused by the following reaction (e.g., Langer et al. 1984):



The backward reaction is ineffective in cold-temperature conditions (~ 10 K), and then the abundance of $^{13}\text{C}^+$ should decrease. Ionic and atomic carbons (C^+ and C) are the main parent species of carbon-chain molecules and the low abundance of $^{13}\text{C}^+$ results in deficient ^{13}C isotopologues of carbon-chain molecules. Table 3 summarizes the $^{12}\text{C}/^{13}\text{C}$ ratios of carbon-chain molecules derived in three starless cores: TMC-1 CP; L1521B; and L134N. From table 3, the following tendencies can be inferred:

1. Cyanopolyynes (HC_{2n+1}N) have relatively lower $^{12}\text{C}/^{13}\text{C}$ ratios compared to the other hydrocarbons. Especially, the ^{13}C isotopomers of CCH have high values.
2. The $^{12}\text{C}/^{13}\text{C}$ ratios are different among the dark clouds. The ratios in L134N are relatively low compared to the others.

An explanation for the first point was proposed by Taniguchi et al. (2019b); the high $^{12}\text{C}/^{13}\text{C}$ ratios of CCH seem to be caused by reactions between hydrocarbons (CCH, C_2H_2 , *l, c*- C_3H) and C^+ . The formed ions will go back to CCH through reactions including electrons and H_2 . If $^{13}\text{C}^+$ is diluted by reaction (4), these reactions will produce hydrocarbons with high $^{12}\text{C}/^{13}\text{C}$ ratios. On the other hand, the $^{12}\text{C}/^{13}\text{C}$ ratios of cyanopolyynes do not likely change after their formation.

The second point may be related to the evolution of the starless cores; TMC-1 CP and L1521B are considered to be chemically younger than L134N (e.g., Dickens et al. 2000). Currently, the available data are limited, and such studies have been conducted mainly at TMC-1 CP. Thus, it is difficult to reach firm conclusions. Future high-sensitivity survey observations are needed to reveal the detailed mechanisms causing the dilution of ^{13}C species, which would give information about the chemical relationships among carbon-chain molecules in cold dark clouds.

3.2 Carbon-Chain Species around Low-Mass YSOs

Carbon-chain chemistry around low-mass young stellar objects (YSOs), namely WCCC, has been reviewed in Sakai & Yamamoto (2013), and we do not discuss WCCC in detail. Instead, we summarize observational results published after the review article of Sakai & Yamamoto (2013).

Several survey observations with single-dish telescopes targeting carbon-chain molecules and COMs have been conducted. Graninger et al. (2016) carried out survey observations of CH_3OH and C_4H toward 16 embedded low-mass protostars using the IRAM 30m telescope. A tentative correlation between the gas-phase $\text{C}_4\text{H}/\text{CH}_3\text{OH}$ abundance ratio and the $\text{CH}_4/\text{CH}_3\text{OH}$ abundance ratio in ice was found. At the protostellar stage, the gas-phase C_4H is considered to form from CH_4 sublimated from dust grains (WCCC), whereas the gas-phase CH_3OH is mainly originated from ice mantle (hot corino chemistry). Thus, the suggested tentative correlation between the gas phase and ice mantle supports the scenario of WCCC; sublimation of CH_4 is a trigger of carbon-chain formation in lukewarm gas (e.g., Hassel et al. 2008).

Higuchi et al. (2018) conducted survey observations of CCH, *c*- C_3H_2 , and CH_3OH toward

Table 3 The $^{12}\text{C}/^{13}\text{C}$ ratios of carbon-chain molecules in dark clouds

Species	TMC-1 CP	L1521B	L134N
H^{13}CCCN	$79 \pm 11^{(a)}$	$117 \pm 16^{(b)}$	$61 \pm 9^{(b)}$
HC^{13}CCN	$75 \pm 10^{(a)}$	$115 \pm 16^{(b)}$	$94 \pm 26^{(b)}$
HCC^{13}CN	$55 \pm 7^{(a)}$	$76 \pm 6^{(b)}$	$46 \pm 9^{(b)}$
$\text{H}^{13}\text{CCCCCN}$	$98 \pm 14^{(c)}$		
$\text{HC}^{13}\text{CCCCN}$	$101 \pm 14^{(c)}$		
$\text{HCC}^{13}\text{CCCN}$	$95 \pm 12^{(c)}$		
$\text{HCCC}^{13}\text{CCN}$	$93 \pm 13^{(c)}$		
$\text{HCCCC}^{13}\text{CN}$	$85 \pm 11^{(c)}$		
HC_7N	$73 \pm 21^{(d)}$		
^{13}CCH	$> 250^{(e)}$	$> 271^{(f)}$	$> 142^{(f)}$
C^{13}CH	$> 170^{(e)}$	$252^{+77}_{-48}{}^{(f)}$	$101^{+24}_{-16}{}^{(f)}$
$^{13}\text{CCCCH}$	$141 \pm 15^{(g)}$		
C^{13}CCCH	$97 \pm 9^{(g)}$		
CC^{13}CCH	$82 \pm 5^{(g)}$		
CCC^{13}CH	$118 \pm 8^{(g)}$		
^{13}CCS	$230 \pm 43^{(h)}$		
C^{13}CS	$54 \pm 2^{(h)}$		
$^{13}\text{CCCS}$	$> 206^{(g)}$		
C^{13}CCS	$48 \pm 5^{(g)}$		
CC^{13}CS	$30 - 206^{(g)}$		

Errors indicate the standard deviation.

References: (a) Takano et al. (1998), (b) Taniguchi et al. (2017a), (c) Taniguchi et al. (2016a), (d) Burkhardt et al. (2018) (average value), (e) Sakai et al. (2010), (f) Taniguchi et al. (2019b), (g) Sakai et al. (2013), (h) Sakai et al. (2007).

36 Class 0/I protostars in the Perseus molecular cloud using the IRAM 30m and Nobeyama 45m radio telescopes. They found that the column density ratio of CCH/CH₃OH varies by two orders of magnitudes among the target sources, and the majority of the sources show intermediate characters between hot corino and WCCC. In other words, hot corino and WCCC are at opposite ends of a spectrum and both carbon-chain species and COMs are present around most low-mass protostars. In addition, they found a possible trend that sources with higher CCH/CH₃OH ratios are located near cloud edges or in isolated clouds. Similar trends were suggested by Lefloch et al. (2018) with data taken in the IRAM Large Program “Astrochemical

Surveys At IRAM (ASAI)”. The ASAI program is an unbiased line survey from 80 to 272 GHz toward 10 sources with various evolutionary stages. Lefloch et al. (2018) found a difference in environmental conditions between hot corino and WCCC sources: i.e., inside and outside dense filamentary cloud regions, respectively.

High-angular-resolution observations with interferometers, such as ALMA and NOEMA, have revealed spatial distributions of carbon-chain molecules around low-mass YSOs. Oya et al. (2017) detected both a carbon-chain molecule (CCH) and several COMs toward the low-mass Class 0 protostar L483. They found that the spatial distribution of CCH is different from those of COMs; the CCH emission shows a hole at the protostar position, whereas emission from COMs is concentrated near the protostar. Such emission features are attributed to WCCC and hot corino chemistry, respectively.

Zhang et al. (2018) found that CCH emission traces the outflow cavity with signatures of rotation with respect to the outflow axis toward the NGC 1333 IRAS 4C outflow in the Perseus molecular cloud using ALMA. Tychoniec et al. (2021) analyzed ALMA data set toward 16 protostars and investigated spatial distributions of each molecule. They also found that CCH and *c*-C₃H₂ trace the cavity wall. This could be explained by the fact that the chemistry of the cavity wall is similar to photodissociation region (PDR) chemistry. The cavity walls are created by the illuminated by the stellar FUV and X-ray radiation field, and the PDR-like chemistry dominates cavity walls. The photodissociation of molecules by UV radiation keeps high gas-phase abundances of atomic carbon (C), which is a preferable condition for the formation of hydrocarbons.

Pineda et al. (2020) found a streamer-like structure toward IRAS 03292+3039 in the Perseus star-forming region with NOEMA. Such a streamer may be well traced by carbon-chain molecules such as CCS and HC₃N, if it is considered to be chemically young. The streamer in this source seems to bring fresh gas from outside of the dense core (> 10500 au) down to the central protostar where the disk forms. Thus the properties of such streamers are potentially important for the formation and evolution of protoplanetary disks.

Taking advantage of the characteristics of carbon-chain molecules, we can trace unique features around low-mass YSOs. Rotational-transition lines of carbon-chain molecules are now found to be useful tracers not only in early starless clouds but also around star-forming cores. ALMA Band 1 and the next generation Very Large Array (ngVLA) will cover the 7 mm band or lower frequency bands, which are suitable for observations of carbon-chain molecules, especially longer ones (see figure 6). Future observations using such facilities will offer new insights into the carbon-chain chemistry around protostars, including low-, intermediate-, and high-mass

systems.

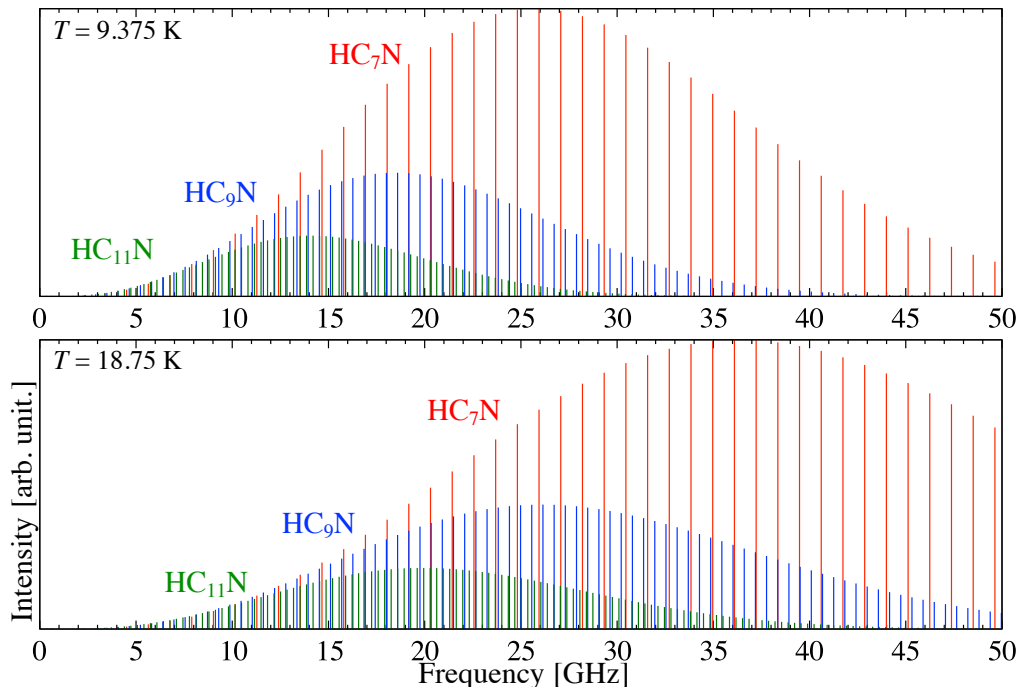


Fig. 6 Predicted line intensities of long cyanopolynes (red; HC₇N, blue; HC₉N, and green; HC₁₁N) in the frequency range of 0 – 50 GHz. The upper and lower panels show predictions at temperatures of 9.375 K and 18.75 K, respectively. The data on rest frequency and line intensity are taken from the CDMS database. Longer carbon-chain species show intensity peaks at lower frequencies.

3.3 Carbon-Chain Species in High-Mass Star-Forming Regions

3.3.1 Chemical Evolutionary Indicators

As mentioned in section 1.2, carbon-chain molecules classically have been known to be abundant in young starless cores and good chemical evolutionary indicators in low-mass star-forming regions. However, it was unclear whether carbon-chain species can be used as chemical evolutionary indicators in high-mass star-forming regions and behave similarly as in the case of low-mass regions.

Survey observations of several carbon-chain species (HC₃N, HC₅N, CCS, and *c*-C₃H₂) and N₂H⁺ were carried out using the Nobeyama 45m radio telescope (Taniguchi et al. 2018a, 2019c). Taniguchi et al. (2018a) observed the HC₃N and HC₅N lines in the 42–45 GHz band toward 17 high-mass starless cores (HMSCs) and 35 high-mass protostellar objects (HMPOs), and

Taniguchi et al. (2019c) observed HC_3N , N_2H^+ , CCS, and $c\text{-C}_3\text{H}_2$ in the 81–94 GHz band toward 17 HMSCs and 28 HMPOs. They proposed the column density ratio of $N(\text{N}_2\text{H}^+)/N(\text{HC}_3\text{N})$ as a chemical evolutionary indicator in high-mass star-forming regions (figure 7). This column density ratio decreases as cores evolve from the starless (HMSC) to protostellar (HMPOs) stage. Sources that were categorized as HMSCs based on the infrared (IR) observations but that are associated with molecular lines of COMs (CH_3OH or CH_3CN) and/or SiO (plotted as the blue diamond in figure 7) tend to fall between HMSCs and HMPOs. These sources are considered to contain early-stage protostars in the dense, dusty cores, which are not easily detected with IR observations. Thus, these sources appear to be at an intermediate evolutionary stage between HMSCs and HMPOs. It is essential to study the physical and chemical features of these sources in detail because they possess information on the initial conditions of high-mass protostars.

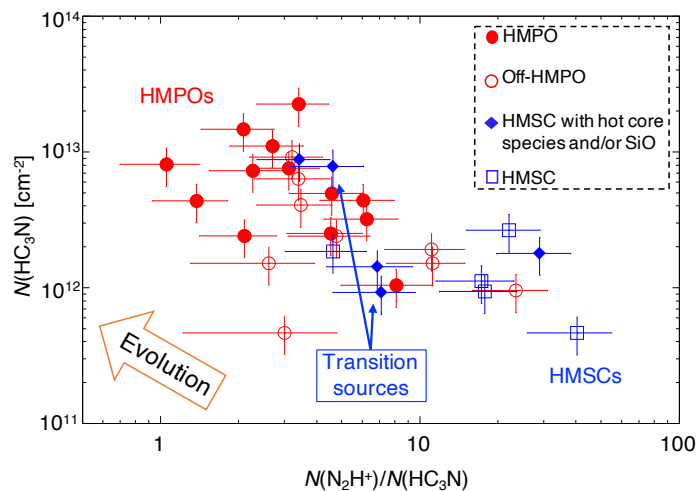


Fig. 7 A chemical evolutionary indicator in high-mass star-forming regions (Taniguchi et al. 2019c). Off-HMPO means that IRAS-observed positions were not at exact continuum peak positions, but the beam covered the continuum core in the beam edge. Blue diamond plots are sources that were identified as HMSCs based on the IR observations, but which are associated with molecular emission lines of COMs (CH_3OH and/or CH_3CN) or SiO.

The decrease of the $N(\text{N}_2\text{H}^+)/N(\text{HC}_3\text{N})$ ratio means that HC_3N is efficiently formed and N_2H^+ is destroyed, as cores evolve. It is a notable point that the tendency of this column density ratio is opposite to that in low-mass star-forming regions (Suzuki et al. 1992; Benson et al. 1998). This tendency could be explained by higher temperatures and extended warm regions around HMPOs compared to low-mass protostars. N_2H^+ is destroyed by a reaction with CO, i.e., abundant in the gas phase after being desorbed from dust grains, and HC_3N

can be formed by CH_4 via the WCCC mechanism or via C_2H_2 desorbed from dust grains. The desorption of CO , CH_4 , and C_2H_2 from dust grains occurs when temperatures reach around 20 K, 25 K, and 50 K, respectively. In summary, the gas-phase chemical composition is affected by the local heating from young massive protostars, and a chemical evolutionary indicator apparently shows an opposite trend compared to that of the low-mass case. Thus, carbon-chain species likely have the potential to become chemical evolutionary indicators even for high-mass protostars.

3.3.2 Cyanopolyynes around High-Mass Protostars

The survey observations mentioned in section 3.3.1 show a possibility of different carbon-chain chemistry between high-mass and low-mass star-forming regions. The detection rates of HC_3N , HC_5N , $c\text{-C}_3\text{H}_2$, CCS are 93%, 50%, 68%, and 46%, respectively, in high-mass star-forming regions (Taniguchi et al. 2018a, 2019c). Law et al. (2018) conducted survey observations toward 16 Class 0/I low-mass protostars with the IRAM 30m telescope and reported that the detection rates of HC_3N , HC_5N , $l\text{-C}_3\text{H}$, C_4H , CCS , and C_3S are 75%, 31%, 81%, 88%, 88%, and 38%, respectively. Thus, cyanopolyynes (HC_3N and HC_5N) show higher detection rates, while CCS is relatively deficient in high-mass star-forming regions compared to low-mass regions. These results imply that carbon-chain chemistry around MYSOs is different from WCCC found around low-mass YSOs.

Taniguchi et al. (2017b) conducted observations of the multi-transition lines of HC_5N using the Green Bank 100m and Nobeyama 45m radio telescopes toward four MYSOs. The derived rotational temperatures are $\sim 20 - 25$ K, which are similar to the temperature regimes of the WCCC mechanism. However, the derived rotational temperatures are lower limits due to contamination from extended cold components covered by the single-dish telescopes. The MYSO G28.28-0.36 shows a particularly unique chemical character: carbon-chain species are rich, but COMs are deficient (Taniguchi et al. 2018b). This source may be analogous to the WCCC source L1527. These results are suggestive of the chemical diversity around MYSOs, as similar to low-mass cases (hot corino and WCCC).

Since the above HC_5N excitation temperatures derived with single-dish data are lower limits due to contamination of cold outer envelopes, it could not be concluded that carbon-chain molecules exist in higher temperature regions around MYSOs compared to the WCCC sources. Taniguchi et al. (2021) derived the $\text{CCH}/\text{HC}_5\text{N}$ abundance ratios toward three MYSOs and compared the observed ratio with the results of their chemical simulations to constrain temperature regimes where carbon-chain species exist. The $\text{CCH}/\text{HC}_5\text{N}$ abundance ratio is

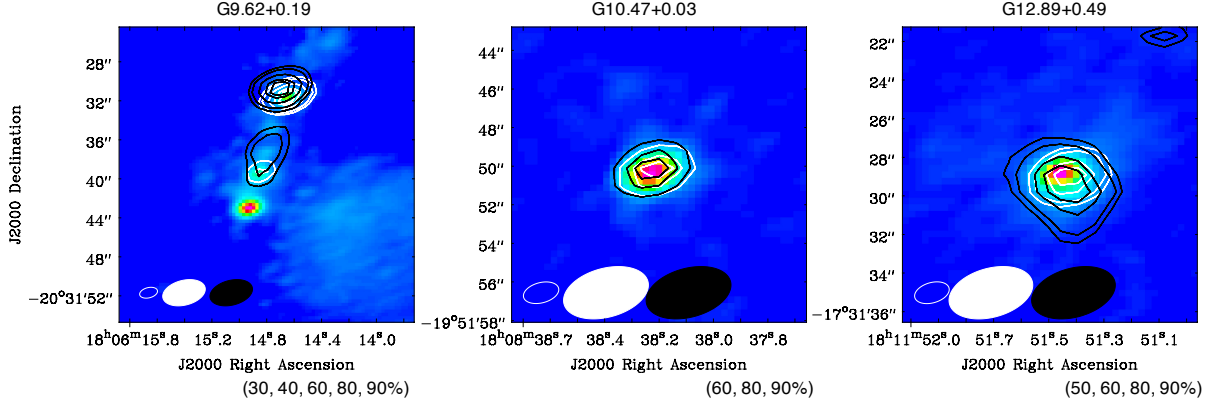


Fig. 8 Comparison of spatial distributions around MYSOs obtained by ALMA (color scale; continuum image, white contours; the CH_3OH line ($1_{0,1} - 2_{1,2}$, $v_t = 1$; $E_{\text{up}} = 302.9$ K), black lines; the HC_5N line ($J = 35 - 34$; $E_{\text{up}} = 80.5$ K). This figure is a modified version of Taniguchi et al. (2023). The contour levels are relative values of the peak intensities, and the contour levels are indicated below each panel. The ellipses at the bottom of each panel indicate the angular resolutions; open one corresponds to the continuum images, and white and black ones correspond to the moment 0 maps of CH_3OH and HC_5N , respectively.

predicted to decrease as the temperature increases, because CCH shows a peak abundance in the gas phase around 30 K, while the gas-phase HC_5N abundance increases as the temperature rises up to ~ 100 K (Taniguchi et al. 2019a). Details about the chemical simulations are presented in section 4. The observed CCH/ HC_5N abundance ratios toward all of the three MYSOs are ~ 15 , which is much lower than that toward the low-mass WCCC source L1527 (625_{-339}^{+3041}). The observed abundance ratios around MYSOs agree with the simulations around 85 K, while the ratio in L1527 matches with the simulations around 35 K. Therefore, carbon-chain species, at least HC_5N , around MYSOs appear to exist in higher temperature regions than the locations where the WCCC mechanism occurs. Such results indicate that carbon-chain chemistry around MYSOs may be different from the WCCC mechanism. It is necessary to reveal spatial distributions of carbon-chain molecules around MYSOs to confirm that the carbon-chain chemistry around MYSOs is different from WCCC.

More recently, spatial distributions of the HC_5N line ($J = 35 - 34$; $E_{\text{up}} = 80.5$ K) around MYSOs have been revealed by ALMA Band 3 data (Taniguchi et al. 2023). This line has been detected from three sources among five target sources. Figure 8 shows the comparison of spatial distributions among HC_5N , CH_3OH , and continuum emission in Band 3 toward the three MYSOs. The HC_5N emission shows single peaks associated with the continuum peaks

and is consistent with the emission of the CH_3OH line ($1_{0,1} - 2_{1,2}$, $v_t = 1$; $E_{\text{up}} = 302.9$ K) which should trace hot core regions with temperatures above 100 K. These results also support the “Hot Carbon-Chain Chemistry” scenario; HC_5N desorbs from dust grains with temperatures above 100 K and shows gas-phase peak abundances similar to those of COMs.

In short, carbon-chain molecules are formed even around MYSOs. However, the WCCC mechanism does not match the observational results around MYSOs, and carbon-chain species, especially cyanopolyynes, exist in hot regions with temperatures above 100 K. Figure 9 shows a summary of chemical properties found around low-mass and high-mass YSOs, respectively. Currently, a candidate of pure HCCC sources is the MYSO G28.28-0.36, in which COMs are deficient but HC_5N is abundant (Taniguchi et al. 2018b). Despite the small source sample, we can see different chemical features among MYSOs. To statistically study the chemical diversity around MYSOs, we need larger source samples obtained by high-angular-resolution observations of carbon-chain species and COMs.

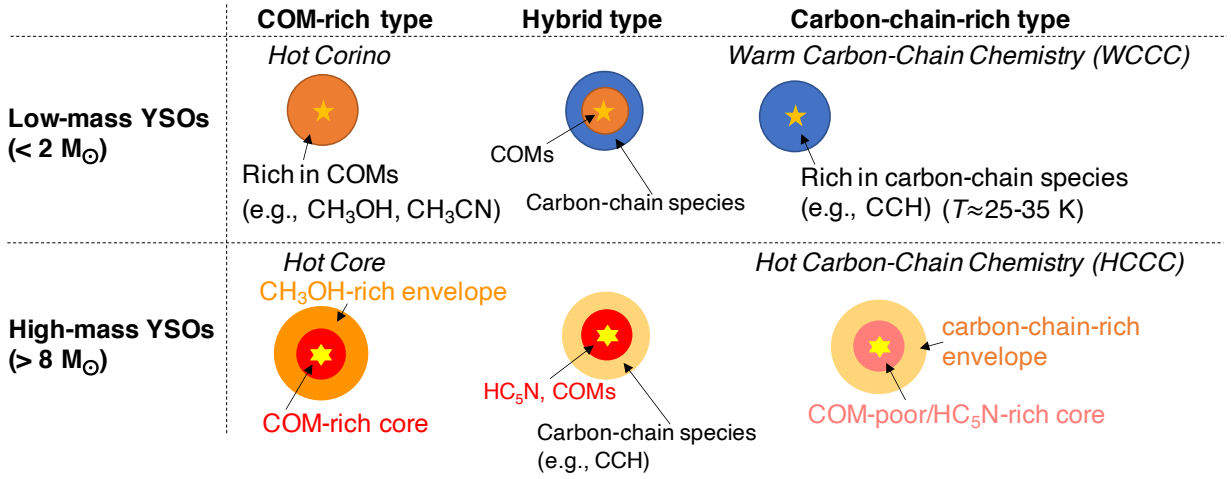


Fig. 9 Chemical properties found around low-mass and high-mass YSO.

3.3.3 Carbon-chains around Intermediate-Mass Protostars

Observations have revealed WCCC and HCCC in low-mass and high-mass star-forming regions, respectively. However, the carbon-chain chemistry around intermediate-mass protostars ($2 M_{\odot} < m_{*} < 8 M_{\odot}$) has not been well studied. Studies to investigate the chemical composition around intermediate-mass protostars are essential to understand the carbon-chain chemistry around protostars comprehensively because large physical gaps between low-mass and high-mass protostars prevent us to compare them straightforwardly.

Survey observations of several carbon-chain molecules in the Q band have been conducted with the Yebes 40m telescope. Twelve target intermediate-mass YSOs were selected from the source list of the SOFIA Massive (SOMA) Star Formation Survey project (De Buizer et al. 2017; Liu et al. 2019). We briefly demonstrate the initial results here.

Table 4 summarizes the detection of molecules toward eleven intermediate-mass protostars. No lines have been detected from one of the target sources, and we exclude it from Table 4. In addition to carbon-chain molecules, several COMs and sulfur-bearing species have also been detected. We have derived the rotational temperatures using seven HC₅N lines (from $J = 12 - 11$ to $J = 18 - 17$; $E_{\text{up}} = 9.97 \text{ K} - 21.9 \text{ K}$). The derived rotational temperatures are around 20 K, which agrees with the WCCC mechanism. In the fitting procedure, we note that the $J = 12 - 11$ line cannot be fitted simultaneously, with the flux of this line being too high. This may indicate the presence of multiple-temperature components: i.e., the $J = 12 - 11$ line may trace mainly cold outer gas that is a remnant of the larger-scale molecular cloud, while the other lines may trace lukewarm gas where carbon-chain molecules efficiently form by the WCCC mechanism. To confirm this, we need results of lower- J transition lines. COMs and carbon-chain molecules have been found around all of the intermediate-mass protostars, indicating that hybrid-type sources are also common in the intermediate-mass regime. Details of this project will be presented in a future paper (K. Taniguchi et al., in preparation).

In summary, carbon-chain formation occurs around intermediate-mass protostars, as well as low-mass and high-mass protostars. Future detail analysis combined with physical parameters and observations with interferometers will reveal whether the HCCC mechanism occurs around intermediate-mass protostars.

Table 4 Summary of initial results of molecules around intermediate-mass protostars

Species	Cepheus E	L1206	HH288	IRAS 00420	IRAS 20343	IRAS 00259	IRAS 05380	IRAS 20293	IRAS 21307	IRAS 22198	IRAS 23385
HC ₃ N	✓	✓	✓	✓	✓	✓	✓	✓	✓	✓	✓
HC ₅ N	✓	✓	✓	✓	✓	✓		✓		✓	✓
C ₃ H		✓	✓	✓		✓				✓	
C ₄ H	✓	✓	✓	✓	✓	✓	✓		✓	✓	✓
<i>l</i> -H ₂ CCC	✓	✓	✓	✓	✓					✓	✓
<i>c</i> -C ₃ H ₂	✓	✓	✓	✓	✓	✓		✓		✓	✓
CCS	✓	✓	✓	✓	✓	✓	✓	✓		✓	✓
C ₃ S	✓	✓	✓	✓	✓					✓	
CH ₃ CCH		✓	✓		✓			✓		✓	
CH ₃ OH	✓	✓	✓	✓	✓	✓		✓	✓	✓	✓
CH ₃ CHO	✓	✓	✓	✓	✓	✓		✓		✓	
H ₂ CCO	✓	✓	✓	✓	✓	✓				✓	
HNCO	✓	✓	✓	✓	✓	✓		✓		✓	
CH ₃ CN	✓	✓	✓	✓	✓	✓				✓	
¹³ CS	✓	✓	✓	✓	✓	✓		✓	✓	✓	✓
C ³⁴ S	✓	✓	✓	✓	✓	✓		✓	✓	✓	✓
HCS ⁺	✓	✓	✓	✓	✓	✓		✓	✓	✓	✓
H ₂ CS	✓	✓	✓	✓	✓	✓		✓	✓	✓	✓

The “✓” mark indicates detection with S/N ratios above 5.

3.4 Carbon-Chain Species in Disks

Before the ALMA era, there were only a few reported detections of carbon-chain species in the protoplanetary disks around T Tauri stars and Herbig Ae stars. Henning et al. (2010) detected CCH from two T Tauri stars, DM Tau and LkCa 15, with the IRAM Plateau de Bure Interferometer (PdBI). The first detection of HC₃N from protoplanetary disks was achieved using the IRAM 30m telescope and PdBI (Chapillon et al. 2012). They detected the HC₃N lines ($J = 12 - 11$ and $16 - 15$) from protoplanetary disks around two T Tauri stars, GO Tau and LkCa 15, and the Herbig Ae star MWC 480. Studies of disk chemistry have dramatically progressed, thanks to ALMA observations. In this subsection, we summarize studies related to carbon-chain species in protoplanetary disks.

Qi et al. (2013) reported the first detection of *c*-C₃H₂ in a disk around the Herbig Ae star HD 163296 using the ALMA Science Verification data. Its emission is consistent with the Keplerian rotating disk and traces a ring structure from an inner radius of ~ 30 au to an outer radius of ~ 165 au. The HC₃N line ($J = 27 - 26$; $E_{\text{up}} = 165$ K) has been detected from the protoplanetary disk of MWC 480, which is a Herbig Ae star in the Taurus region, using ALMA (Öberg et al. 2015). Angular resolutions are $0.4'' - 0.6''$, corresponding to 50–70 au. The data can spatially resolve the molecular emission, and show a velocity gradient caused by Keplerian rotation of the protoplanetary disk. Öberg et al. (2015) also detected CH₃CN and H¹³CN in the same observation, and found that the abundance ratios among the three species in the protoplanetary disk of MWC 480 are different from those in the solar-type protostellar binary system IRAS 16293-2422. Thus, they suggested that varying conditions among protoplanetary disks can lead to chemical diversity in terms of carbon-chain species.

Bergner et al. (2018) conducted survey observations of CH₃CN and HC₃N toward four T Tauri stars (AS 209, IM Lup, LkCa 15, and V4046 Sgr) and two Herbig Ae stars (MWC 480 and HD 163296) with ALMA. Typical angular resolutions are from $\sim 0.5''$ to $\sim 1.5''$. They detected the HC₃N ($J = 27 - 26$) line from all of their target sources. Besides, the $J = 31 - 30$ and $J = 32 - 31$ lines have been detected from MWC 480. The spatial distributions of HC₃N and CH₃CN show similarity; compact and typically well within the bounds of the dust continuum. HC₃N is considered to be formed by only the gas-phase reactions: C₂H₂ + CN and CCH + HNC (see also table 2).

The Molecules with ALMA at Planet-forming Scales (MAPS) ALMA Large Program has studied disk chemistry around five target sources (IM Lup, GM Aur, AS 209, HD 163296, and MWC 480) in Bands 3 and 6 (Öberg et al. 2021). Typical beam sizes are around $0.3''$ and $0.1''$ in

Band 3 and Band 6, respectively. Ilee et al. (2021) presented the results for HC_3N , CH_3CN , and $c\text{-C}_3\text{H}_2$. The HC_3N and $c\text{-C}_3\text{H}_2$ lines have been clearly detected from four of the target sources, with the exception being IM Lup, where only one $c\text{-C}_3\text{H}_2$ line has been tentatively detected. The $c\text{-C}_3\text{H}_2$ emission shows clear ring-like features in AS 209, HD 163296, and MWC 480, suggestive of an association with the outer dust rings. Two HC_3N lines ($J = 11 - 10$ and $29 - 28$) show ring-like distributions in AS 209 and HD 163296, whereas the $J = 29 - 28$ line appears centrally peaked in MWC 480. The HC_3N emission of the $J = 11 - 10$ line is similarly extended to that of $c\text{-C}_3\text{H}_2$, but the $J = 29 - 28$ line seems to be more compact. CH_3CN , on the contrary, appears to have a ring-like feature only in AS 209, while more centrally peaked structures are seen in the other sources. Ilee et al. (2021) demonstrated that the observed HC_3N emission traces upper layers ($z/r = 0.1 - 0.4$) of the protoplanetary disks compared to that of CH_3CN ($z/r \leq 0.1 - 0.2$). They also found that the $\text{HC}_3\text{N}/\text{HCN}$ and $\text{CH}_3\text{CN}/\text{HCN}$ abundance ratios of the outer regions (50–100 au) in the target disks are consistent with the composition of cometary materials. The warmer disks, HD 163296 and MWC 480, likely have comet formation zones at correspondingly larger radii.

Guzmán et al. (2021) presented distributions of CCH toward the five protoplanetary disks of the MAPS program. They proposed that the CCH emission comes from relatively warmer (20–60 K) layers. In HD 163296, there is a decrease in the column density of CCH and HCN inside of the dust gaps near ~ 83 au, at which a planet has been considered to be located. The similar spatial distributions of CCH and HCN suggest that they are produced by the same chemical processes, and photochemistry is the most probable one.

ALMA observations have revealed the presence of disks around not only T Tauri and Herbig Ae stars, but also around more massive, O-/B-type stars. Csengeri et al. (2018) detected the vibrationally-excited HC_3N line ($J = 38 - 37$, $v_7 = 1e$) around the O-type star G328.2551-0.5321 (O5–O4 type star) with ALMA. This source is a high-mass protostar in the main accretion phase. Their data have spatial resolution of around 400 au. The position-velocity (PV) diagram of this HC_3N vibrationally-excited line is consistent with a Keplerian disk rotation profile, and they proposed that such HC_3N vibrationally-excited emission could be a new tracer for compact accretion disks around high-mass protostars.

Taniguchi et al. (2022) detected the HC_3N vibrationally-excited lines ($J = 24 - 23$, $v_7 = 2, l = 0$ and $2e$) from the hypercompact H_{II} (HC H_{II}) region G24.47-0.08 A1 using ALMA Band 6 data. Their emission morphologies are largely similar to those of CH_3CN , which was suggested to trace Keplerian disk rotation around a central mass of $20 M_\odot$ in the previous study of Moscadelli et al. (2021). The column densities of HC_3N and CH_3CN were derived using lines of

their ^{13}C isotopologues, and the $\text{CH}_3\text{CN}/\text{HC}_3\text{N}$ abundance ratios were compared with those in protoplanetary disks around the lower-mass stars obtained by the MAPS program (Ilee et al. 2021). Figure 10 shows the comparisons of the $\text{CH}_3\text{CN}/\text{HC}_3\text{N}$ abundance ratios in disks. It is clear that the ratio in the disk around the G24 HC H_{II} region is higher than those around the lower-mass stars by more than one order of magnitude.

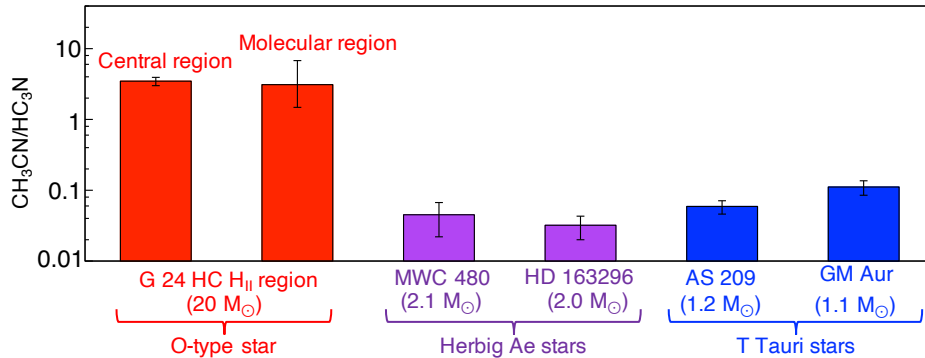


Fig. 10 Comparison of the $\text{CH}_3\text{CN}/\text{HC}_3\text{N}$ abundance ratios in disks around various stellar masses, which is modified from Taniguchi et al. (2022). Results of Herbig Ae and T Tauri stars are from Ilee et al. (2021).

Such a difference in the $\text{CH}_3\text{CN}/\text{HC}_3\text{N}$ abundance ratio was explained by the HC_3N and CH_3CN chemistry in the disk: efficient thermal sublimation of CH_3CN from ice mantles and rapid destruction of HC_3N by the UV photodissociation and/or reactions with ions (H^+ , H_3^+ , HCO^+). In the protoplanetary disks, CH_3CN is considered to be efficiently formed by dust-surface reactions: (1) the successive hydrogenation reactions of C_2N ; and (2) a radical-radical reaction between CH_3 and CN (Loomis et al. 2018a). The derived excitation temperature of CH_3CN in the G24 HC H_{II} region ($T_{\text{ex}} \approx 335$ K) is much higher than its sublimation temperature (~ 95 K), which suggests that CH_3CN formed on dust surfaces efficiently sublimates by the thermal desorption mechanism. On the other hand, its excitation temperatures around the Herbig Ae and T Tauri stars were derived to be 30–60 K, which is suggestive of the non-thermal desorption mechanisms such as photodesorption (Loomis et al. 2018a; Ilee et al. 2021). This means that CH_3CN sublimation is not efficient in disks around the Herbig Ae and T Tauri stars, leading to low gas-phase abundances of CH_3CN . Both HC_3N and CH_3CN could be destroyed by the UV radiation, and the UV photodissociation rate of HC_3N is higher than that of CH_3CN by a factor of ~ 2.4 (Le Gal et al. 2019). Thus, HC_3N could be more rapidly destroyed by UV photodissociation. In addition, HC_3N is destroyed by reactions with ions,

which are expected to be abundant in the H_{II} region. In summary, HC_3N is likely destroyed rapidly in the G24 $HC H_{II}$ region.

Until now, there is only one O-type star disk in which the CH_3CN/HC_3N abundance ratio has been derived. We need similar data for an increased sample of sources, including T Tauri, Herbig Ae, and O/B type disks, including probing various evolutionary stages, to further test the apparent tentative trends that have been so far revealed. In addition, for such studies of disk structures, especially around the more distant massive protostars, it is important to conduct unbiased line survey observations with high angular resolution.

3.5 Carbon-Chain Species in Other Environments

Carbon-chain molecules have been detected not only from star-forming regions in our Galaxy, but also other environments of the ISM. We briefly summarize the carbon-chain species detected in these regions.

Small hydrocarbons have been known to be present in photodissociation regions (PDRs). Cuadrado et al. (2015) observed small hydrocarbons toward the Orion Bar PDR using the IRAM 30m telescope. They detected various small hydrocarbons (CCH , C_4H , $c-C_3H_2$, $c-C_3H$, $C^{13}CH$, ^{13}CCH , $l-C_3H$, and $l-H_2C_3$) and the $l-C_3H^+$ ion. They found that the spatial distributions of CCH and $c-C_3H_2$ are similar but do not follow the PAH emission, and suggested that photo-destruction of PAHs is not a necessary requirement for the observed abundances of the smallest hydrocarbons. Instead, the gas-phase reactions between C^+ and H_2 produce the small hydrocarbons. Guzmán et al. (2015) observed small hydrocarbons (CCH , $c-C_3H_2$), $l-C_3H^+$, and DCO^+ toward the Horsehead PDR with the PdBI. They demonstrated that top-down chemistry, in which large polyatomic molecules or small carbonaceous grains are photo-destroyed into smaller hydrocarbon molecules or precursors, works in this PDR. Suggestions by these two studies (Cuadrado et al. 2015; Guzmán et al. 2015) seem in contradiction but may imply that the carbon-chain chemistry in PDRs differs among regions. Thus, further study is needed of carbon-chain chemistry in PDRs.

The envelopes of the carbon-rich Asymptotic Giant Branched (AGB) star IRC+10216 are known as a carbon-chain-rich site. Several carbon-chain molecules have been discovered for the first time in this source in both radio and infrared regimes (see also section 2.3). For example, diacetylene (C_4H_2) has been detected in mid-infrared observations with the 3m Infrared Telescope Facility (IRTF) from this source (Fonfría et al. 2018). This molecule is distributed in two populations with different excitation conditions; cold and hot rotational temperatures

were derived to be 47 ± 7 K and 420 ± 120 K, respectively.

Pardo et al. (2022) conducted deep line survey observations in the Q band with the Yebes 40m telescope and summarized the detected carbon-chain species in this source. The rotational temperatures of the carbon-chain species are around 5–25 K, suggesting that carbon-chain species may exist in different regions. The species detected with the radio telescope exist in colder regions compared to the species detected with the infrared telescope. There remain a lot of unidentified lines (U lines), and future laboratory spectroscopic experiments are necessary for line identifications.

The planetary nebula CRL 618, another carbon-chain-rich source, has been studied by radio and infrared observations. Polyacetylenic chains (C_4H_2 and C_6H_2) and benzene (C_6H_6) have been detected here with the Infrared Space Observatory (ISO) (Cernicharo et al. 2001). The abundances of C_4H_2 and C_6H_2 are lower than that of C_2H_2 by only a factor of 2–4, while benzene is less abundant than acetylene by a factor of ~ 40 . These authors suggested that UV photons from the hot central star and shocks associated with its high-velocity winds affect the chemistry in CRL 618: i.e., the UV photons and shocks drive the polymerization of acetylene and the formation of benzene. These hydrocarbons likely survive in harsh regions compared to star-forming regions. Pardo et al. (2005) observed cyanopolyynes up to HC_7N , and proposed rapid transformation from small cyanide to longer cyanopolyynes in this source.

Berné & Tielens (2012) investigated formation process of C_{60} by the infrared observations with *Spitzer* and *Herschel* toward the NGC 7023 reflection nebula. They found that C_{60} is efficiently formed in cold environments of an interstellar cloud irradiated by the strong UV radiation field. The most plausible formation route is the photochemical processing of large PAHs.

Carbon-rich AGB stars or planetary nebulae, like IRC+10216 and CRL 618, appear to possess unique carbon-chain chemistry differing from that in star-forming regions and PDRs, and thus be important laboratories to study carbon chemistry, including PAHs and benzene. Future observations with infrared telescopes, such as James Webb Space Telescope (JWST), may give us new insights of carbon chemistry, in particular carbonaceous dust grains, PAHs, and fullerenes. In fact, recent observations with JWST have revealed the presence of dust shells around the Wolf-Rayet binary WR 140, which likely implies an episodic dust formation process (Lau et al. 2022). Using JWST, we can also reveal the spatial distributions of PAHs and fullerenes, as well as dust grains. Similar observations will be able to be applied for C-rich AGB stars or planetary nebulae and reveal the carbon chemistry around these harsh environments. Furthermore, we can investigate relationships among carbon-chain species, hy-

drocarbons, fullerenes, and carbonaceous dust by a combination of ALMA and JWST. These studies are essential to reveal what forms of carbon are ejected into the ISM and how they are incorporated into future star formation events. This point will be essential to reveal the origin of large carbon-chain molecules and species including benzene rings that have been recently detected at TMC-1 CP (section 3.1.1).

ALMA observations have detected carbon-chain species in extragalactic sources. The ALMA Comprehensive High-resolution Extragalactic Molecular Inventory (ALCHEMI) large program has conducted line survey observations from 84.2 GHz to 373.2 GHz toward the starburst galaxy NGC 253. Several carbon-chain species (e.g., CCH, *c*-C₃H₂, HC₃N, HC₅N, HC₇N, CCS) have been detected from this galaxy (Martín et al. 2021). The detection of more complex carbon-chain species will be reported (Dr. Sergio Martin, ESO/JAO, private comm.). Shimonishi et al. (2020) detected CCH in a hot molecular core in the Large Magellanic Cloud (LMC), and found that the CCH emission traces outflow cavity, as also seen in the low-mass YSOs in our Galaxy (see section 3.2). Such observations toward extragalactic sources with different metallicities will be important for a comprehensive understanding of carbon chemistry in the ISM.

Summaries of this section are as follows:

1. Recent line survey observations toward TMC-1 by the Green Bank 100m and Yebes 40m telescopes discovered various and unexpected carbon-chain molecules. However, abundances of some of them cannot be explained by chemical simulations, meaning that our current knowledge about carbon chemistry in the ISM lacks important processes.
2. Survey observations toward low-mass YSOs revealed that both carbon-chain species and COMs are present around most of the low-mass YSOs. Hot corino and WCCC states are likely to be extreme ends of a continuous distribution.
3. Since carbon-chain molecules trace chemically young gas, their lines can be powerful tracers of streamers, which are important structures to understand star formation and disk evolution.
4. Carbon-chain species are formed around MYSOs. ALMA observations have shown that they exist in hot core regions with temperatures above 100 K. Thus, the carbon-chain chemistry is not the WCCC mechanism found around low-mass YSOs, but rather indicates the presence of “Hot Carbon-Chain Chemistry (HCCC)”.
5. The vibrationally-excited lines of HC₃N can be used as a disk tracer around massive stars. The disk chemistry around massive stars may be different from that around lower-mass stars (i.e., T Tauri and Herbig Ae stars), although there is the need to increase the source samples

to confirm this.

6. Infrared observations toward carbon-rich AGB stars and planetary nebulae have detected polyacetylene chains, benzene, and fullerenes in their envelopes. These sites are unique laboratories to study carbon chemistry which is different from that in star-forming regions.
7. Beyond our Galaxy, several carbon-chain species have also been detected in other galaxies enabled by high-sensitivity ALMA observations.

4 Chemical Simulations

Modeling studies about carbon-chain chemistry in starless cores have tried to obtain good agreement with the observed abundances in the dark cloud TMC-1. Here, we review modeling studies covering various types of carbon-chain molecules in dark clouds.

Loison et al. (2014) studied several carbon-chain groups (C_n , C_nH , C_nH_2 , $C_{2n+1}O$, C_nN , $HC_{2n+1}N$, $C_{2n}H^-$, C_3N^-) with gas-grain chemical models including updated reaction rate constants and branching ratios assuming two different C/O ratios (0.7 and 0.95). They added a total of 8 new species and 41 new reactions, and modified 122 rate coefficients taken from the KInetic Database for Astrochemistry (KIDA, kida.uva.2011). Their results clearly show that some carbon-chain molecules depend on the C/O elemental abundance ratio (e.g., C_nH where $n = 4, 5, 6, 8$). Their models with new parameters can obtain good agreement with the observed abundances in the dark cloud TMC-1 CP, and the models with two C/O ratios (0.7 and 0.95) obtain a similar agreement at different times. There are two ages that show better agreement between observations and models; 10^5 yr and around $(1 - 2) \times 10^6$ yr. The gas-phase chemistry is dominated at the earlier phase, whereas the grain surface chemistry and gas-grain interaction become more efficient at the later stages because of more frequent collisions between gas-phase particles and dust grains.

These authors also compared the modeled results to the observed abundances in another starless core, L134N. Here the models with a C/O ratio of 0.7 are in better agreement with the observed abundances compared to the case with the higher C/O ratio. Ages when the models agree with the observed abundances in L134N best are $(3 - 5) \times 10^4$ yr and $\sim 6 \times 10^5$ yr. Large amounts of free C, N, and O are available in the gas phase at the first age, while strong depletion effects are predicted at the later stage. They also suggested that experimental work for the determination of rate constants for the reactions of $O + C_nH$ and $N + C_nH$, especially at low-temperature conditions, is necessary.

Most recent studies have focused on particular molecules that were newly detected at

TMC-1 CP (section 3.1.1). Classical models for dark clouds consider bottom-up chemistry starting from C^+ , with carbon-chain molecules considered to form mainly by gas-phase reactions (section 1.2). However, such classical views need to be revisited. For example, it has been revealed that both gas-phase and grain-surface formation routes are important for the reproduction of the observed abundance of H_2CCCHC_3N (Shingledecker et al. 2021). Some molecules detected by the GOTHAM project, especially cyclic molecules, have not been explained by the chemical simulations yet (e.g., *c*- C_9H_8 ; Burkhardt et al. 2021b). These results suggest that small rings are formed through the destruction of PAHs or other unknown processes. Our knowledge about connections among different categories (e.g., linear, cyclic, PAHs) likely lacks important processes. Besides, we need to reveal the initial conditions of carbon-bearing species in molecular clouds. Further observations and chemical simulations are necessary to understand carbon-chain chemistry including the newly detected molecules.

Some recent studies with sophisticated chemical simulations focused on the origin of the chemical diversity around YSOs. Aikawa et al. (2020) demonstrated their results with two phases (the static phase and the collapse phase) and a multilayered ice mantle model, and investigated how the WCCC and hot corino chemistry depend on the physical conditions during the static phase. They found:

1. The lower temperatures ($T \leq 15$ K) during the static phase can produce the WCCC sources more efficiently.
2. The lower visual extinction during the static phase can form CH_4 and carbon-chain molecules become more abundant.
3. A longer static phase is preferable for producing the WCCC sources.
4. It is difficult to produce the prototypical WCCC sources, where carbon-chain species are rich but COMs are deficient. On the contrary, the hot corino sources and hybrid-type sources where both COMs and carbon-chain species are reasonably abundant could be reproduced.

In warm conditions, grain-surface formation and freeze out of CH_4 , which is a key species for WCCC, become less effective. Moreover, the conversion of CO to CO_2 on grain surfaces becomes important, and the gaseous CO abundance decreases. These lead to a low abundance of C^+ , which is formed by the destruction of CO by He^+ . The C^+ ion is another key species for WCCC. Therefore, warm conditions are not suitable for the production of WCCC sources. In the model with a longer static phase, CH_4 accumulates during the static phase, leading to a more favorable condition for WCCC.

Kalvāns (2021) investigated the effects of the UV radiation field and cosmic rays on

the formation of WCCC sources. They concluded that WCCC can be caused by exposure of a star-forming core to the interstellar radiation field (ISRF) or just to cosmic rays (with $\zeta \geq 10^{-16} \text{ s}^{-1}$). Such a conclusion agrees with the observational results that hot corino type sources are located inside dense filamentary clouds, while the WCCC sources are located outside such structures (e.g., Lefloch et al. 2018). These two model studies show that various factors, including conditions before the onset of core collapse, are related to carbon-chain chemistry around low-mass YSOs. These factors likely are entangled in most sources.

Taniguchi et al. (2019a) tried to reproduce the observed abundances of HC_5N around the three MYSOs observed with the single-dish telescopes (section 3.3.2) with chemical simulations of hot-core models with a warm-up period. They utilized three different heating timescales (t_h); $5 \times 10^4 \text{ yr}$, $2 \times 10^5 \text{ yr}$, and $1 \times 10^6 \text{ yr}$, approximating high-mass, intermediate-mass, and low-mass star-formation, respectively (Garrod & Herbst 2006). Figure 11 shows the model results of HC_5N (gas phase, dust surface, and ice mantle) during the warm-up and hot-core periods with a heating timescale of $1 \times 10^6 \text{ yr}$. In figure 11, we indicate the lower limits of the gas-phase HC_5N abundance in two MYSOs; G12.89+0.49 and G28.28-0.36 that show the minimum and maximum abundances, respectively (Taniguchi et al. 2017b). The observed abundances derived by single-dish telescopes are considered to be lower limits due to beam dilution. The observed lower limits of HC_5N around the MYSOs can be reproduced when the temperature reaches its sublimation temperature ($\sim 115 \text{ K}$) or the hot-core phase ($T = 200 \text{ K}$).

These authors also investigated cyanopolyne chemistry in detail during the warm-up and hot-core periods. Basically, formation and destruction reactions of HC_3N , HC_5N , and HC_7N are similar. We give an explanation of HC_5N as an example (figure 11). The gas-phase HC_5N abundance (red curves) shows a drastic change with time (or temperature) evolution. During the warm-up period, HC_5N is mainly formed by the reaction between C_4H_2 and CN . In addition to this, the reaction between CCH and HC_3N partly contributes to the HC_5N formation. This reaction ($\text{CCH} + \text{HC}_3\text{N}$) is important around $t \approx 8.5 \times 10^5 \text{ yr}$, when the gas-phase HC_3N abundance increases. At that time, the HC_3N production is enhanced by the reaction between CCH and HNC . We indicate some molecules with green arrows in figure 11. These indicate that each molecule directly sublimates from dust grains at these various ages. Methane (CH_4) sublimates from dust grains around 25 K ($t \approx 7.2 \times 10^5 \text{ yr}$), and carbon-chain formation starts, namely WCCC. After that, CN and C_2H_2 sublimate from dust grain at $t = 7.7 \times 10^5 \text{ yr}$ ($T \approx 31 \text{ K}$) and $t = 9.3 \times 10^5 \text{ yr}$ ($T \approx 55 \text{ K}$), respectively. The C_4H_2 species is formed by the gas-phase reaction of “ $\text{CCH} + \text{C}_2\text{H}_2 \rightarrow \text{C}_4\text{H}_2 + \text{H}$ ”. When the temperature reaches around 73 K ($t = 1.0 \times 10^6 \text{ yr}$), C_4H_2 directly sublimates from dust grains. The enhancement of the

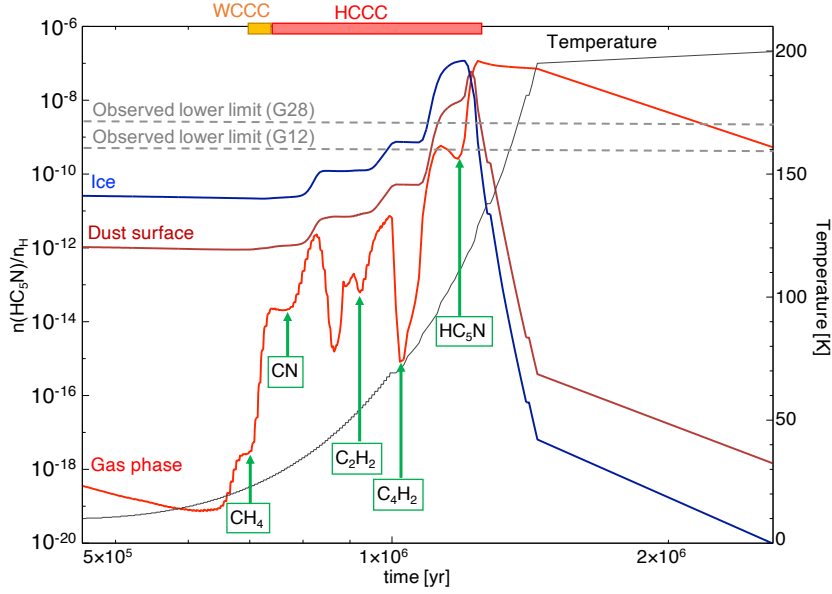


Fig. 11 The modeled HC_5N abundances in the gas phase (red), dust surface (brown), and ice mantle (blue) during the warm-up and hot-core periods (Taniguchi et al. 2019a). The black line indicates the temperature evolution. Indicated molecules mark the times of efficient sublimation from dust grains. The gray horizontal dashed lines indicate the observed lower limits of the gas-phase HC_5N abundances toward two MYSOs; G12.89+0.49 (5×10^{-10}) and G28.28-0.36 (2.1×10^{-9}).

gas-phase abundances of CN and C_4H_2 boosts the formation of HC_5N in the gas phase.

We can see that the HC_5N abundances in dust surface and ice mantles increase when the gas-phase HC_5N abundance decreases. This means that the HC_5N molecules, which are formed in the gas phase, adsorb onto dust grains and accumulate in ice mantles before the temperature reaches its sublimation temperature ($T \approx 115$ K, corresponding to $t = 1.2 \times 10^6$ yr). Taniguchi et al. (2023) have advocated the concept of HCCC (Figure 4) based on these results.

This chemical simulation is supported by observations of the ^{13}C isotopic fractionation (c.f., section 3.1.2) of HC_3N toward the carbon-chain-rich MYSO G28.28-0.36 (Taniguchi et al. 2016b). The proposed main formation pathway of HC_3N is the reaction between C_2H_2 and CN in this MYSO. This is consistent with the formation process seen in the chemical simulations during the warm-up stage.

Taniguchi et al. (2019a) proposed that longer heating timescales of the warm-up stage (t_h) could produce the carbon-chain-rich conditions by comparisons of six modeled results, focusing on cyanopolyynes. In the HCCC mechanism, cyanopolyynes are formed in the gas phase,

adsorb onto dust grains, and accumulate in the ice mantle. Their ice-mantle abundances just before sublimation determine the gas-phase peak abundances. Thus, longer heating timescales allow cyanopolyynes to accumulate in the ice mantle abundantly, leading to their higher gas-phase abundances in hot core regions. The long heating timescale of the warm-up stage (t_h) does not necessarily reflect the timescale of stellar evolution or accretion. It depends on the relationships between the size of the warm region (R_{warm}) and the infall velocity (v_{infall}) as suggested by Aikawa et al. (2008):

$$t_h \propto \frac{R_{\text{warm}}}{v_{\text{infall}}}. \quad (5)$$

If R_{warm} becomes larger or v_{infall} becomes smaller, t_h will be longer. The R_{warm} and v_{infall} values should be related to various physical parameters (e.g., protostellar luminosity, density structure, magnetic field strength). The conditions of R_{warm} and v_{infall} can be investigated by observations. Combined observations to derive chemical composition and the values of $R_{\text{warm}}/v_{\text{infall}}$ are needed for a more comprehensive understanding of the chemical evolution and diversity around YSOs.

5 Theoretical Studies

5.1 Role of Quantum Chemical Studies

Quantum chemistry is an indispensable tool to study structures and spectral properties of a given molecule, regardless of laboratory stability, and makes this a necessary component of astrochemical analyses. It is probably the best tool to explore and interpret chemical structures, properties, and, most importantly, detectable spectra of unusual molecules detected in space. In the 1960s and 1970s, when radio telescopes came into action with better sensitivity, many species were identified based on the laboratory data of their rotational spectra. However, there were also many unidentified signatures. Closed shell molecules can be easily handled in the laboratory and generate rotational spectra. The problem arises in the case of radical and charged species because of their highly unstable and reactive nature. Initial detection of HCO^+ and N_2H^+ was in the 1970s and based on quantum chemistry (see Fortenberry 2015, and references therein). Following these, Patrick Thaddeus (Columbia University and then Harvard University) was a part of teams that detected nearly three dozen new molecular species (McCarthy & Thaddeus 2001). Thaddeus' group standardized the use of quantum chemistry in astrochemical detection.

Several carbon-chain species such C_2H , C_3N , and C_4H were identified based on SCF (self-consistent field) computation. The usage of quantum chemistry in astrochemistry became popular and common if species had not been synthesized in a laboratory. Several carbon-chain

species, such as $l\text{-C}_3\text{H}^+$ and C_6H^- , were identified based on the insight of quantum chemistry. This has continued until recent times with the detection of the kentenyl radical (HCCO) towards various dark clouds in 2015. In another example, the detection of C_5N^- in the circumstellar envelope of the carbon-rich star IRC+10216 was based solely on quantum chemical data.

Modern quantum computations consider a lot of improvements with a wide range of quantum mechanical methods, basis sets, especially coupled cluster theory, at the single, double, and perturbative triples [CCSD(T)] level. The CCSD(T) method is exceptionally good at providing molecular structures and rotational constants, which provide reference rotational spectra. The CCSD(T) method is considered the gold standard in quantum chemical calculations to obtain accurate bond energies and molecular properties (e.g., Ramabhadran & Raghavachari 2013; Fortenberry 2015; Barone et al. 2015; Fortenberry 2017). Over the years, many groups have made remarkable contributions to astrochemistry through quantum chemistry for astrochemical detection, understanding of the formation/destruction, and collisional excitation of different interstellar molecules (e.g., groups led by L. Allamandola, C. Bauschlicher, N. Balucani, V. Barone, M. Biczysko, P. Botschwina, R. C. Fortenberry, J. Gauss, J. Kästner, T. J. Lee, J-C Loison, K. Peterson, C. Puzzarini, A. Rimola, H. F. Schaefer, J. Stanton, P. Ugliengo, D. Woon). A comprehensive strategy for treating larger molecules with the required accuracy has been presented by Barone et al. (2015).

5.1.1 Ground State and Stability

The ground states of carbon-chain species are crucial because they decide their stability and eventually help us find the true state of the species either in laboratory experiments or in astrophysical environments via a spectral search. Table 1 summarizes the ground state of all the carbon-chain species included in this review article. The ground state, enthalpy of formation, rotational constants, dipole moment, and polarizability of many carbon-chain species can be found in KIDA database (<https://kida.astrochem-tools.org/>) as well as in several works in the literature (e.g., Woon & Herbst 2009; Etim et al. 2016; Etim & Arunan 2017; Bâldea 2019; Etim et al. 2020). For any particular carbon-chain species, the ground state can be found with the help of quantum chemical study.

5.1.2 Dipole moment and Polarizability

The dipole moment is an important parameter that decides whether a molecule is polar or non-polar. Non-polar molecules do not have a permanent electric dipole moment and do not show rotational transitions. On the other hand, polar molecules have a permanent electric dipole

moment and they show rotational transitions. A higher dipole moment value means a higher intensity of rotational transitions. It is crucial because one can say whether it is detectable or not through their rotational transitions. In addition to the symmetry of molecules, several other factors are important for their detectability in interstellar environments. These factors include the density of spectral lines, the partition functions, and the intrinsic line strengths of the transitions. The dipole moment values of all the carbon-chain species are summarized in table 1. These can be measured theoretically with various quantum chemical methods and basis set by inclusion of structures of molecules.

The polarizabilities of all carbon-chain species, if available, are summarized in table 1. The dipole moment and polarizability are crucial for the estimation of ion-neutral reaction rates. Ion-neutral reactions play a crucial role in the ISM, especially in cold dark clouds, for the formation and destruction of various species. For non-polar neutrals, the rate coefficient is given by the so-called Langevin expression:

$$k_L = 2\pi e \sqrt{\frac{\alpha_{\text{pola}}}{\mu}}, \quad (6)$$

where e is the electronic charge, α_{pola} is the polarizability, μ is the reduced mass of reactants, and cgs-esu units are utilized so that the units for the rate coefficient are $\text{cm}^3 \text{s}^{-1}$. For polar-neutral species, trajectory scaling relation is usually used. The best-known formula for the ion-dipolar rate coefficient k_D in the classical regime and for linear neutrals is the Su-Chesnavich expression. The Su-Chesnavich (Su & Chesnavich 1982) formula is based on the parameter x , defined by

$$x = \frac{\mu_D}{\sqrt{2\alpha_{\text{pola}}k_B T}}, \quad (7)$$

where μ_D is an effective dipole moment of the neutral reactant, which is generally very close to the true dipole moment, and k_B is the Boltzmann constant. The larger value of x takes, the larger the rate coefficient is.

Apart from the estimation of the rate coefficient of ion-neutral reactions, the dipole moment is one of the key parameters to determine the column density of observed species. Accurate estimation of the dipole moments is essential to derive realistic values of column density. For instance, the dipole moment of C_4H was used ~ 0.87 Debye in previous literature, which was the value of mixed states, i.e., ground and excited states. The recent result suggests the dipole moment value is 2.10 Debye, which is 2.4 times larger than the values used before (Oyama et al. 2020). As a result, its column densities have been overestimated by a factor of ~ 6 .

5.1.3 Binding Energy of Carbon-Chain Species

A major portion of carbon-chain species is primarily formed in the gas phase. In addition, gas-grain exchange occurs, and many reactions occur on the grain surface. The binding energy (BE) plays a pivotal role in interstellar chemistry, especially grain surface chemistry, which eventually enriches the gas-phase chemistry. Here, we describe the role of binding energy in interstellar chemical processes.

The BE values of all carbon-chain species are provided (if available) in table 5. Most of the BE values are mainly taken from KIDA (<https://kida.astrochem-tools.org/>). BE estimation of a species heavily depends on the methods and surface used for the calculations (e.g., Penteado et al. 2017; Das et al. 2018; Ferrero et al. 2020; Villadsen et al. 2022; Minissale et al. 2022). The BE values of all carbon-chain species, especially higher-order linear chains, are estimated based on the addition method that are provided in KIDA. In this method, for instance, the BE of HC₇N is estimated by addition of binding energies of HC₆N and C. 800 K is usually adopted as the BE of a carbon atom. However, we see a huge difference in BE of a carbon atom between the old value and newly measured values based on quantum chemical study (≥ 10000 K; Wakelam et al. 2017; Minissale et al. 2022). Thus, the addition method of BE may lead to large uncertainties to estimate BE of carbon-chain molecules, especially longer ones. If BE of a carbon atom is $\geq 10,000$ K is correct, the addition method of BE may not be valid, because long carbon-chain species will have huge BE values. To overcome this issue, dedicated quantum chemical calculations or the temperature-programmed desorption (TPD) method are required to estimate the BE values of carbon-chain species with higher accuracy.

Gas-phase species accrete onto the grain surface depending upon their energy barriers with the surfaces. The species may bind to the grain surface via the physisorbed or chemisorbed processes. E_d expresses the binding energy (or desorption energy) of the chemical species. Species attached to grain surfaces can migrate from one site to another depending on the barrier energy of migration (E_b). This is also known as a barrier against diffusion. The migration timescale by thermal hopping can be expressed as,

$$t_{\text{hop}} = \nu_0^{-1} \exp\left(\frac{E_b}{k_B T_d}\right) \text{ s}, \quad (8)$$

where ν_0 is the characteristic vibration frequency of the adsorbed species, and T_d is the grain surface temperature. The theoretical expression for ν_0 is,

$$\nu_0 = \sqrt{\frac{2n_s E_d}{\pi^2 m}} \text{ s}^{-1}, \quad (9)$$

where m is the mass of the adsorbed particle, and n_s is the number density of sites. The utilized

values of n_s are $\sim 2 \times 10^{14} \text{ cm}^{-2}$ for olivine based grain and $\sim 5 \times 10^{13} \text{ cm}^{-2}$ for the amorphous carbon grain, respectively (Biham et al. 2001). The characteristic frequency is $\sim 10^{12}$ Hz. Diffusion time t_{diff} required for an adsorbed particle over a number of sites is given by

$$t_{\text{diff}} = N t_{\text{hop}} S, \quad (10)$$

where S is the total number of sites on the grain surface.

Desorption is the release of species on the grain surface back into the gas phase. There are various desorption mechanisms that directly depend on the binding energy of the species. For instance, the thermal evaporation time of species on a grain surface is given by,

$$t_{\text{evap}} = \nu^{-1} \exp\left(\frac{E_d}{k_B T_d}\right) \text{ s.} \quad (11)$$

Species on the grain surface attain sufficient thermal energy and evaporate from the surface after this characteristic time. Therefore, the thermal desorption rate can be written as

$$K_{\text{evap,A}} = \nu \exp\left(-\frac{E_{\text{bind,A}}}{k_B T}\right), \quad (12)$$

where ν is the characteristics frequency that can be written as,

$$\nu = \sqrt{\frac{2N_s E_{\text{bind,A}}}{\pi^2 m_A}}, \quad (13)$$

where N_s is the density of the binding site, and m_A is the mass of species A. The binding energy of the chemical species and the evaporation rate can be estimated from TPD experiments. Thermal desorption is a very efficient mechanism in hot cores, hot corinos, and other dense and high-temperature locations of star-forming regions.

6 Experimental Studies

Experimental studies are essential to measure the rotational or vibrational spectra of molecules with unprecedented resolution and accuracy. They can provide accurate molecular rotational spectra, which are used for their precise identification in data obtained from various radio and infrared telescopes. The first carbon-chain molecule, the simplest cyanopolyne HC_3N , was detected with NRAO 140-foot radio telescope in 1971 based on the laboratory rotational spectra measured by Tyler & Sheridan (1963). After that, the astronomical detection of many carbon-chain species was based on their laboratory rotational spectra. References to laboratory experiments of rotational or vibrational spectra of different molecules can be found in papers reporting their interstellar detection.

Here we describe a few studies of carbon-chain species, mainly focusing on molecules containing a benzene ring. The first benzene ring (C_6H_6) and its cyano derivative, benzonitrile

(*c*-C₆H₅CN) were detected toward CRL 618 and TMC-1, respectively, based on their laboratory infrared and rotational spectra (e.g., McGuire et al. 2018). The most striking and groundbreaking results, the detection of fullerenes (C₆₀, C₇₀) and its protonated form C₆₀⁺ was also based on their laboratory data (e.g., Martin et al. 1993; Nemes et al. 1994; Kato et al. 1991). In the 2020s, several PAHs have been identified in the ISM with the aid of their laboratory spectra. For instance, two isomers of cyanonaphthalene (McGuire et al. 2021; McNaughton et al. 2018), two isomers of ethynyl cyclopentadiene (McCarthy et al. 2021; Cernicharo et al. 2021d; McCarthy et al. 2020), 2-cyanoindene (Sita et al. 2022), fulvenallene (McCarthy et al. 2020; Sakaizumi et al. 1993b), ethynyl cyclopropenylidene, cyclopentadiene, and indene (Cernicharo et al. 2021b; Burkhardt et al. 2021b, and references therein).

Laboratory experiments to investigate reactions have also been developed. Experimental investigations of carbon-bearing molecule formation via neutral-neutral reactions are summarized in Kaiser (2002). Ion-molecule reactions producing carbon-chain species were also investigated via experiments (Takagi et al. 1999; Žabka et al. 2014). Recently, Martínez et al. (2020) investigated the growth of carbon-containing species from C and H₂ in conditions analogous of circumstellar envelopes around carbon-rich AGB stars. They found that nanometer-sized carbon particles, pure carbon clusters, and aliphatic carbon species are formed efficiently, whereas aromatics are generated at trace levels and no fullerenes are detected. They also suggested that the formation of aromatic species must occur via other processes, such as the thermal processing of aliphatic material on the surface of dust grains.

7 Summary and Open Questions of This Review

7.1 Summary

We have reviewed carbon-chain chemistry in the ISM, mainly focusing on recent updates. A summary of our main points is as follows.

1. By the end of 2022, 118 carbon-chain species have been detected in the ISM. This accounts for almost 44% of 270 interstellar molecules detected in the ISM or circumstellar shells. These include various families of carbon-chain species, involving elements of O, N, S, P, and Mg.
2. Two line survey projects toward TMC-1 CP (GOTHAM and QUIJOTE) have recently reported detections of many new carbon-chain species. Abundances of some of these species are not yet reproducible in chemical simulations indicating a need for improved models.
3. In addition to the cold gas conditions of early-phase molecular clouds, carbon-chain for-

mation also occurs around low-, intermediate- and high-mass YSOs. Warm Carbon-Chain Chemistry (WCCC) was found in 2008 around low-mass YSOs, while Hot Carbon-Chain Chemistry (HCCC) has been proposed based on observations around high-mass YSOs recently.

4. Chemical simulations aim to explain conditions forming hot corino and WCCC sources. There are several possible parameters to reproduce the chemical differentiation: e.g., UV radiation field and temperature during the static phase.
5. Thanks to high-angular resolution and high-sensitivity observations with ALMA, several carbon-chain species (e.g., CCH, *c*-C₃H₂, HC₃N) have been detected from protoplanetary disks around Herbig Ae and T Tauri stars. Vibrationally-excited lines of HC₃N have been found to trace disk structures around massive stars.
6. Circumstellar envelopes around carbon-rich AGB stars and planetary nebulae are unique factories of carbon chemistry. Infrared observations have revealed the presence of PAHs and fullerenes in such environments. Recent laboratory experiments investigated chemistry in such regions.
7. Carbon-chain species have been detected even in extragalactic environments, such as the starburst galaxy NGC253 via the ALCHEMI project. In the Large Magellanic Cloud (LMC), CCH emission has been found to trace outflow cavities, as seen in low-mass YSOs in our Galaxy.
8. Theoretical and experimental studies are important for the observational detection of carbon-chain species and for obtaining an understanding of their formation and destruction processes. Developments of these techniques are important to reveal carbon-chain chemistry in various physical conditions in the ISM.

The presence of carbon-chain species in the ISM has been known since the early 1970s, and many researchers have investigated their features through observations, chemical simulations, laboratory experiments, and quantum calculations. Recent findings raise new questions about carbon-chain chemistry, and it is an exciting time of progress. To solve the newly raised questions, collaborative research involving observations, laboratory experiments, and chemical simulations is crucial.

To understand the carbon-chain chemistry better by observational methods, we need more dedicated low-frequency, high-sensitivity, and high angular resolution observations towards dark clouds, low- and high-mass YSOs, and other environments. In the near future, ALMA Band 1, ngVLA and the Square Kilometer Array (SKA) will become available. Observations using these facilities will be essential to reveal links between ISM physics and

carbon-chain chemistry, the origin of chemical differentiation around YSOs, and relationships between WCCC and HCCC. In addition, future observational studies combining infrared data (e.g., from JWST, Thirty Meter Telescope (TMT), European Extremely Large Telescope (E-ELT)) and radio (ALMA, ngVLA, SKA, and future single-dish) telescopes have the potential from breakthrough results. For instance, relationships between PAHs/small dust grains and common carbon-chain species, which can be observed by infrared and radio regimes, respectively, can be studied by such a combination.

7.2 Open Key Questions

Recent new discoveries of carbon-chain molecules in the ISM have raised new questions, and we have realized that our knowledge about carbon-chain chemistry is far from complete. We highlight the following open questions:

1. How do large carbon-chain species, which have been found in TMC-1 CP, form? Is there a role for both bottom-up and top-down processes?
2. How are PAHs and fullerenes related to other carbon-chain species in the ISM?
3. In what form is the main carbon reservoir ejected into the ISM? How does it propagate into the ISM and become incorporated into molecular clouds where the next-generation of star formation occurs?
4. Which, if any, important formation/destruction processes of carbon-chain species are missing from current chemical models?
5. Can we estimate more accurate branching ratios for different species (e.g., isomers) in electron recombination reactions?
6. How can we obtain accurate binding energy of carbon-chain species?
7. Are there reactions forming and/or destroying carbon-chain species on dust surfaces and within ice mantles?

Answers to these questions likely require combined efforts of multi-wavelength observational, theoretical, and experimental study.

Acknowledgments

K.T. is grateful to Professor Eric Herbst (University of Virginia) for leading me to the astrochemical field, working with me, and giving a lot of comments on studies of carbon-chain molecules that are presented in this article. K.T. appreciates Professor Masao Saito (National Astronomical Observatory of Japan) for giving his advice and continuous encouragement. K.T. is supported by JSPS KAKENHI grant No.JP20K14523. P. G acknowledges the support from the Chalmers Initiative of Cosmic Origins Postdoctoral Fellowship. We thank Professor Fumitaka Nakamura (National Astronomical Observatory of Japan) and Professor

Table 5 Binding energy of carbon-chain species

Species	Binding energy (K)	Species	Binding energy (K)	Species	Binding energy (K)
C ₂	10000	C ₈ N	7200	C ₃ O	2750
C ₃	2500	C ₉ N	8000	C ₅ O	4350
C ₄	3200	C ₁₀ N	8800	C ₇ O	5950
C ₅	4000	C ₂ H ₂	2587	C ₉ O	7550
C ₆	4800	C ₂ H ₄	2500	HC ₂ O	2400
C ₇	5600	C ₂ H ₅	3100	SiC ₂	4300
C ₈	6400	C ₂ H ₆	1600	SiC ₃	5100
C ₉	7200	C ₄ H ₂	4187	SiC ₄	5900
C ₁₀	8000	C ₅ H ₂	4987		
C ₁₁	9600	C ₆ H ₂	5787		
C ₂ H	3000	C ₇ H ₂	6587		
<i>l</i> -C ₃ H	4000	C ₂ P	4300		
<i>c</i> -C ₃ H	5200	C ₃ P	5900		
C ₄ H	3737	C ₄ P	7500		
C ₅ H	4537	C ₂ S	2700		
C ₆ H	5337	C ₃ S	3500		
C ₇ H	6137	C ₄ S	4300		
C ₈ H	6937	HC ₃ N	4580		
<i>c</i> -C ₃ H ₂	5900	HC ₄ N	5380		
C ₂ N	2400	HC ₅ N	6180		
C ₃ N	3200	HC ₆ N	7780		
C ₄ N	4000	HC ₇ N	7780		
C ₅ N	4800	HC ₈ N	9380		
C ₆ N	5600	HC ₉ N	9380		
C ₇ N	6400	C ₂ O	1950		

Taken from the KIDA (<https://kida.astrochem-tools.org/>), and also see Wakelam et al. (2017), Penteadó et al. (2017), Das et al. (2018).

Kazuhito Dobashi (Tokyo Gakugei University) for providing original data of mapping observations of carbon-chain species toward TMC-1 obtained by the Nobeyama 45m radio telescope. We would also like to thank Dr. Emmanuel E. Etim for his comments and suggestions. J.C.T. acknowledges support from ERC Advanced Grant MSTAR. We appreciate Dr. Ryan Lau for his comments and suggestions.

References

- Adams, N. G., Smith, D., Giles, K., & Herbst, E. 1989, *A&A*, 220, 269
- Agúndez, M., Cernicharo, J., & Guélin, M. 2014, *A&A*, 570, A45
- . 2015, *A&A*, 577, L5
- Aikawa, Y., Furuya, K., Yamamoto, S., & Sakai, N. 2020, *ApJ*, 897, 110
- Aikawa, Y., Wakelam, V., Garrod, R. T., & Herbst, E. 2008, *ApJ*, 674, 984
- Anderson, J. K., & Ziurys, L. M. 2014, *ApJL*, 795, L1
- Apponi, A. J., McCarthy, M. C., Gottlieb, C. A., & Thaddeus, P. 1999, *ApJL*, 516, L103
- Asplund, M., Grevesse, N., Sauval, A. J., & Scott, P. 2009, *ARA&A*, 47, 481
- Avery, L. W., Broten, N. W., MacLeod, J. M., Oka, T., & Kroto, H. W. 1976, *ApJL*, 205, L173
- Bâldea, I. 2019, *Advanced Theory and Simulations*, 2, 1900084
- Barone, V., Biczysko, M., & Puzzarini, C. 2015, *Accounts of chemical research*, 48, 1413
- Benson, P. J., Caselli, P., & Myers, P. C. 1998, *ApJ*, 506, 743
- Bergner, J. B., Guzmán, V. G., Öberg, K. I., Loomis, R. A., & Pegues, J. 2018, *ApJ*, 857, 69
- Bernath, P. F., Hinkle, K. H., & Keady, J. J. 1989, *Science*, 244, 562
- Berné, O., & Tielens, A. G. G. M. 2012, *Proceedings of the National Academy of Science*, 109, 401
- Biham, O., Furman, I., Pirronello, V., & Vidali, G. 2001, *ApJ*, 553, 595
- Blanksby, S. J., McAnoy, A. M., Dua, S., & Bowie, J. H. 2001, *Monthly Notices of the Royal Astronomical Society*, 328, 89
- Botschwina, P. 1987, *Chemical Physics Letters*, 139, 255
- . 1991, *The Journal of Chemical Physics*, 95, 4360
- . 1993, *Journal of physical chemistry*, 99, 6217
- Broten, N. W., Oka, T., Avery, L. W., MacLeod, J. M., & Kroto, H. W. 1978, *ApJL*, 223, L105
- Brown, R. D., Eastwood, F. W., Elmes, P. S., & Godfrey, P. D. 1983, *Journal of the American Chemical Society*, 105, 6496
- Brünken, S., Gupta, H., Gottlieb, C. A., McCarthy, M. C., & Thaddeus, P. 2007, *ApJL*, 664, L43
- Buhl, D., & Snyder, L. E. 1973, in *Molecules in the Galactic Environment*, ed. M. A. Gordon & L. E. Snyder, 187
- Burkhardt, A. M., Herbst, E., Kalenskii, S. V., et al. 2018, *Monthly Notices of the Royal Astronomical Society*, 474, 5068
- Burkhardt, A. M., Loomis, R. A., Shingledecker, C. N., et al. 2021a, *Nature Astronomy*, 5, 181
- Burkhardt, A. M., Long Kelvin Lee, K., Bryan Changala, P., et al. 2021b, *ApJL*, 913, L18
- Cabezas, C., Agúndez, M., Marcelino, N., et al. 2022a, *A&A*, 659, L8
- . 2022b, *A&A*, 657, L4

Cami, J., Bernard-Salas, J., Peeters, E., & Malek, S. E. 2010, *Science*, 329, 1180

Caminati, W. 1993, *Journal of the Chemical Society, Faraday Transactions*, 89, 4153

Campbell, E. K., Holz, M., Gerlich, D., & Maier, J. P. 2015, *Nature*, 523, 322

Caselli, P., & Ceccarelli, C. 2012, *aapr*, 20, 56

Caselli, P., Pineda, J. E., Sipilä, O., et al. 2022, *ApJ*, 929, 13

Cernicharo, J., Agúndez, M., Cabezas, C., et al. 2021a, *A&A*, 656, L21

—. 2021b, *A&A*, 649, L15

Cernicharo, J., Agúndez, M., Kaiser, R. I., et al. 2021c, *A&A*, 652, L9

—. 2021d, *A&A*, 655, L1

Cernicharo, J., Cabezas, C., Endo, Y., et al. 2021e, *A&A*, 646, L3

Cernicharo, J., Fuentetaja, R., Cabezas, C., et al. 2022a, *A&A*, 663, L5

Cernicharo, J., & Guélin, M. 1996, *A&A*, 309, L27

Cernicharo, J., Guélin, M., Agúndez, M., et al. 2007, *A&A*, 467, L37

Cernicharo, J., Guélin, M., Agúndez, M., McCarthy, M. C., & Thaddeus, P. 2008, *ApJL*, 688, L83

Cernicharo, J., Guélin, M., & Pardo, J. R. 2004, *ApJL*, 615, L145

Cernicharo, J., Heras, A. M., Tielens, A. G. G. M., et al. 2001, *ApJL*, 546, L123

Cernicharo, J., Kahane, C., Gomez-Gonzalez, J., & Guélin, M. 1986, *A&A*, 164, L1

Cernicharo, J., Marcelino, N., Agúndez, M., et al. 2020a, *A&A*, 642, L8

—. 2020b, *A&A*, 642, L17

Cernicharo, J., Marcelino, N., Pardo, J. R., et al. 2020c, *A&A*, 641, L9

Cernicharo, J., Cabezas, C., Pardo, J. R., et al. 2019, *A&A*, 630, L2

Cernicharo, J., Cabezas, C., Agúndez, M., et al. 2021f, *A&A*, 648, L3

Cernicharo, J., Agúndez, M., Cabezas, C., et al. 2022b, *A&A*, 657, L16

Cernicharo, J., Fuentetaja, R., Agúndez, M., et al. 2022c, *A&A*, 663, L9

Chantzos, J., Rivilla, V. M., Vasyunin, A., et al. 2020, *A&A*, 633, A54

Chapillon, E., Dutrey, A., Guilloteau, S., et al. 2012, *ApJ*, 756, 58

Choe, J. C. 2021, *ApJ*, 914, 136

Compagnon, I., Antoine, R., Broyer, M., et al. 2001, *Phys. Rev. A*, 64, 025201

Cordiner, M. A., Charnley, S. B., Kisiel, Z., McGuire, B. A., & Kuan, Y. J. 2017, *ApJ*, 850, 187

Cox, A. P., Ewart, I. C., & Stigliani, W. M. 1975, *Journal of the Chemical Society, Faraday Transactions 2: Molecular and Chemical Physics*, 71, 504

Crawford, T. D., Stanton, J. F., Saeh, J. C., & Schaefer, H. F. 1999, *Journal of the American Chemical Society*, 121, 1902

Csengeri, T., Bontemps, S., Wyrowski, F., et al. 2018, *A&A*, 617, A89

Cuadrado, S., Goicoechea, J. R., Pilleri, P., et al. 2015, *A&A*, 575, A82

Dalgarno, A. 2008, *The Annual Review of Astronomy and Astrophysics*, 46, 1

Das, A., Sil, M., Gorai, P., Chakrabarti, S. i. K., & Loison, J. C. 2018, *ApJS*, 237, 9

De Buizer, J. M., Liu, M., Tan, J. C., et al. 2017, *ApJ*, 843, 33

Dickens, J. E., Irvine, W. M., Snell, R. L., et al. 2000, *ApJ*, 542, 870

Dobashi, K., Shimoikura, T., Nakamura, F., et al. 2018, *ApJ*, 864, 82

Dobashi, K., Shimoikura, T., Ochiai, T., et al. 2019, *ApJ*, 879, 88

Etim, E. E., & Arunan, E. 2017, *Ap&SS*, 362, 4

Etim, E. E., Gorai, P., Das, A., Chakrabarti, S. K., & Arunan, E. 2016, *ApJ*, 832, 144

Etim, E. E., Gorai, P., Ghosh, R., & Das, A. 2020, *Spectrochimica Acta Part A: Molecular Spectroscopy*, 230, 118011

Ewing, D. 1989, *Journal of the American Chemical Society*, 111, 8809

Ferrero, S., Zamirri, L., Ceccarelli, C., et al. 2020, *ApJ*, 904, 11

Foing, B. H., & Ehrenfreund, P. 1994, *nat*, 369, 296

Fonfría, J. P., Agúndez, M., Cernicharo, J., Richter, M. J., & Lacy, J. H. 2018, *ApJ*, 852, 80

Fortenberry, R. C. 2015, *Journal of Physical Chemistry A*, 119, 9941

Fortenberry, R. C. 2017, *International Journal of Quantum Chemistry*, 117, 81

Friberg, P., Hjalmarsen, A., Guelin, M., & Irvine, W. M. 1980, *ApJL*, 241, L99

Frisch, M. J., Trucks, G. W., Schlegel, H. B., et al. 2013, *Gaussian 09 Revision D.01*, gaussian Inc. Wallingford CT

Fuentetaja, R., Agúndez, M., Cabezas, C., et al. 2022a, *A&A*, 667, L4

Fuentetaja, R., Cabezas, C., Agúndez, M., et al. 2022b, *A&A*, 663, L3

Furuya, K., Aikawa, Y., Sakai, N., & Yamamoto, S. 2011, *ApJ*, 731, 38

Garrod, R. T., & Herbst, E. 2006, *A&A*, 457, 927

Ghiasi, R., & Monnajemi, M. 2006, *Journal of the Korean Chemical Society*, 50, 281

Gordon, V. D., McCarthy, M., Apponi, A., & Thaddeus, P. 2002, *ApJS*, 138, 297

Graedel, T. E., Langer, W. D., & Frerking, M. A. 1982, *ApJS*, 48, 321

Graninger, D. M., Wilkins, O. H., & Öberg, K. I. 2016, *ApJ*, 819, 140

Guelin, M., & Cernicharo, J. 1991, *A&A*, 244, L21

Guelin, M., Green, S., & Thaddeus, P. 1978, *ApJL*, 224, L27

Guelin, M., Neining, N., & Cernicharo, J. 1998, *A&A*, 335, L1

Guelin, M., & Thaddeus, P. 1977, *ApJL*, 212, L81

Guelin, M., Cernicharo, J., Travers, M. J., et al. 1997, *A&A*, 317, L1

Guzmán, V. V., Pety, J., Goicoechea, J. R., et al. 2015, *ApJL*, 800, L33

Guzmán, V. V., Bergner, J. B., Law, C. J., et al. 2021, *ApJS*, 257, 6

Halfen, D. T., Clouthier, D. J., & Ziurys, L. M. 2008, *ApJL*, 677, L101

Hassel, G. E., Herbst, E., & Garrod, R. T. 2008, *ApJ*, 681, 1385

Henning, T., Semenov, D., Guilloteau, S., et al. 2010, *ApJ*, 714, 1511

Herbst, E. 1983, *ApJS*, 53, 41

Herbst, E., Adams, N. G., & Smith, D. 1983, *ApJ*, 269, 329

Herbst, E., Smith, D., & Adams, N. G. 1984, *A&A*, 138, L13

Herbst, E., & van Dishoeck, E. F. 2009, *The Annual Review of Astronomy and Astrophysics*, 47, 427

Higuchi, A. E., Sakai, N., Watanabe, Y., et al. 2018, *ApJS*, 236, 52

Hinkle, K. W., Keady, J. J., & Bernath, P. F. 1988, *Science*, 241, 1319

Hirano, T., Nakagawa, N., Murakami, A., & Nomura, O. 1989, *Chemical Physics Letters*, 162, 89

Hollenbach, D., & Salpeter, E. E. 1971, *ApJ*, 163, 155

Hollis, J. M., Remijan, A. J., Jewell, P. R., & Lovas, F. J. 2006, *ApJ*, 642, 933

Ilee, J. D., Walsh, C., Booth, A. S., et al. 2021, *ApJS*, 257, 9

Irvine, W. M., Hoglund, B., Friberg, P., Askne, J., & Ellder, J. 1981, *ApJL*, 248, L113

Jensen, S. S., Jørgensen, J. K., Kristensen, L. E., et al. 2019, *A&A*, 631, A25

Jørgensen, J. K., Belloche, A., & Garrod, R. T. 2020, *The Annual Review of Astronomy and Astrophysics*, 58, 727

Kaifu, N., Suzuki, H., Ohishi, M., et al. 1987, *ApJL*, 317, L111

Kaifu, N., Ohishi, M., Kawaguchi, K., et al. 2004, *pasj*, 56, 69

Kaiser, R. I. 2002, *Chemical Reviews*, 102, 1309

Kalvāns, J. 2021, *ApJ*, 910, 54

Kato, T., Kodama, T., Shida, T., et al. 1991, *Chemical Physics Letters*, 180, 446

Kawaguchi, K., Kasai, Y., Ishikawa, S.-I., et al. 1994, *ApJL*, 420, L95

Kawaguchi, K., Takano, S., Ohishi, M., et al. 1992, *ApJL*, 396, L49

Kraka, E., & Cremer, D. 1993, *Chemical Physics Letters*, 216, 333

Kroto, H. W., Kirby, C., Walton, D. R. M., et al. 1978, *ApJS*, 219, L133

Langer, W. D., Graedel, T. E., Frerking, M. A., & Armentrout, P. B. 1984, *ApJ*, 277, 581

Langer, W. D., Velusamy, T., Kuiper, T. B. H., et al. 1997, *ApJL*, 480, L63

Lau, R. M., Hankins, M. J., Han, Y., et al. 2022, *Nature Astronomy*, 6, 1308

Laurie, V. W. 1956, *The Journal of Chemical Physics*, 24, 635

Law, C. J., Öberg, K. I., Bergner, J. B., & Graninger, D. 2018, *ApJ*, 863, 88

Le Gal, R., Brady, M. T., Öberg, K. I., Roueff, E., & Le Petit, F. 2019, *ApJ*, 886, 86

Lee, K. L. K., Changala, P. B., Loomis, R. A., et al. 2021, *ApJL*, 910, L2

- Lefloch, B., Bachiller, R., Ceccarelli, C., et al. 2018, *Monthly Notices of the Royal Astronomical Society*, 477, 4792
- Little, L. T., Riley, P. W., & Matheson, D. N. 1977, *Monthly Notices of the Royal Astronomical Society*, 181, 33P
- Liu, M., Tan, J. C., De Buizer, J. M., et al. 2019, *ApJ*, 874, 16
- Loison, J.-C., Wakelam, V., Hickson, K. M., Bergeat, A., & Mereau, R. 2014, *Monthly Notices of the Royal Astronomical Society*, 437, 930
- Loomis, R. A., Cleeves, L. I., Öberg, K. I., et al. 2018a, *ApJ*, 859, 131
- Loomis, R. A., Öberg, K. I., Andrews, S. M., et al. 2018b, *The Astronomical Journal*, 155, 182
- Loomis, R. A., Burkhardt, A. M., Shingledecker, C. N., et al. 2021, *Nature Astronomy*, 5, 188
- Marcelino, N., Agúndez, M., Tercero, B., et al. 2020, *A&A*, 643, L6
- Martin, M. C., Koller, D., & Mihaly, L. 1993, *Phys. Rev. B*, 47, 14607
- Martín, S., Mangum, J. G., Harada, N., et al. 2021, *A&A*, 656, A46
- Martínez, L., Santoro, G., Merino, P., et al. 2020, *Nature Astronomy*, 4, 97
- Matthews, H. E., Friberg, P., & Irvine, W. M. 1985, *ApJ*, 290, 609
- Matthews, H. E., Irvine, W. M., Friberg, P., Brown, R. D., & Godfrey, P. D. 1984, *nat*, 310, 125
- McCarthy, M. C., Gottlieb, C. A., Gupta, H., & Thaddeus, P. 2006, *ApJL*, 652, L141
- McCarthy, M. C., Lee, K. L. K., Carroll, P. B., et al. 2020, *Journal of Physical Chemistry A*, 124, 5170
- McCarthy, M. C., & Thaddeus, P. 2001, *Chemical society reviews*, 30, 177
- McCarthy, M. C., Lee, K. L. K., Loomis, R. A., et al. 2021, *Nature Astronomy*, 5, 176
- McGuire, B. A. 2022, *ApJS*, 259, 30
- McGuire, B. A., Burkhardt, A. M., Kalenskii, S., et al. 2018, *Science*, 359, 202
- McGuire, B. A., Burkhardt, A. M., Shingledecker, C. N., et al. 2017, *ApJL*, 843, L28
- McGuire, B. A., Burkhardt, A. M., Loomis, R. A., et al. 2020, *ApJL*, 900, L10
- McGuire, B. A., Loomis, R. A., Burkhardt, A. M., et al. 2021, *Science*, 371, 1265
- McNaughton, D., Jahn, M. K., Travers, M. J., et al. 2018, *Monthly Notices of the Royal Astronomical Society*, 476, 5268
- Milam, S. N., Savage, C., Brewster, M. A., Ziurys, L. M., & Wyckoff, S. 2005, *ApJ*, 634, 1126
- Minissale, M., Aikawa, Y., Bergin, E., et al. 2022, *ACS Earth and Space Chemistry*, 6, 597
- Mohamed, S., McCarthy, M., Cooksy, A., Hinton, C., & Thaddeus, P. 2005, *The Journal of chemical physics*, 123, 234301
- Morris, M., Turner, B. E., Palmer, P., & Zuckerman, B. 1976, *ApJ*, 205, 82
- Moscadelli, L., Cesaroni, R., Beltrán, M. T., & Rivilla, V. M. 2021, *A&A*, 650, A142

Nakamura, F., Kamenno, S., Kusune, T., et al. 2019, *pasj*, 71, 117

Nakamura, F., Ogawa, H., Yonekura, Y., et al. 2015, *pasj*, 67, 117

Nemes, L., Ram, R. S., Bernath, P. F., et al. 1994, *Chemical Physics Letters*, 218, 295

Nguyen, T. L., Mebel, A. M., Lin, S. H., & Kaiser, R. I. 2001, *Journal of Physical Chemistry A*, 105, 11549

Öberg, K. I., & Bergin, E. A. 2021, *Physics Reports*, 893, 1

Öberg, K. I., Guzmán, V. V., Furuya, K., et al. 2015, *nat*, 520, 198

Öberg, K. I., Guzmán, V. V., Walsh, C., et al. 2021, *ApJS*, 257, 1

Ohishi, M., Kaifu, N., Kawaguchi, K., et al. 1989, *ApJL*, 345, L83

Ohishi, M., Suzuki, H., Ishikawa, S.-I., et al. 1991, *ApJL*, 380, L39

Oya, Y., Sakai, N., Watanabe, Y., et al. 2017, *ApJ*, 837, 174

Oyama, T., Ozaki, H., Sumiyoshi, Y., et al. 2020, *ApJ*, 890, 39

Pardo, J. R., Cernicharo, J., & Goicoechea, J. R. 2005, *ApJ*, 628, 275

Pardo, J. R., Cernicharo, J., Tercero, B., et al. 2022, *A&A*, 658, A39

Pascoli, G., & Lavendy, H. 1998, *International Journal of Mass Spectrometry*, 181, 11

Penteado, E. M., Walsh, C., & Cuppen, H. M. 2017, *ApJ*, 844, 71

Pety, J., Gratier, P., Guzmán, V., et al. 2012, *A&A*, 548, A68

Pineda, J. E., Segura-Cox, D., Caselli, P., et al. 2020, *Nature Astronomy*, 4, 1158

Prasad, S. S., & Huntress, W. T., J. 1980a, *ApJS*, 43, 1

—. 1980b, *ApJ*, 239, 151

Puzzarini, C. 2008, *Chemical Physics*, 346, 45

Qi, C., Öberg, K. I., Wilner, D. J., & Rosenfeld, K. A. 2013, *ApJL*, 765, L14

Ramabhadran, R. O., & Raghavachari, K. 2013, *Journal of chemical theory and computation*, 9, 3986

Remijan, A., Scolati, H. N., Burkhardt, A. M., et al. 2023, *ApJL*, 944, L45

Remijan, A. J., Hollis, J. M., Lovas, F. J., et al. 2007, *ApJL*, 664, L47

Remijan, A. J., Hollis, J. M., Snyder, L. E., Jewell, P. R., & Lovas, F. J. 2006, *ApJL*, 643, L37

Roueff, E., Felenbok, P., Black, J. H., & Gry, C. 2002, *A&A*, 384, 629

Sakai, N., Ikeda, M., Morita, M., et al. 2007, *ApJ*, 663, 1174

Sakai, N., Sakai, T., Hirota, T., Burton, M., & Yamamoto, S. 2009, *ApJ*, 697, 769

Sakai, N., Sakai, T., Hirota, T., & Yamamoto, S. 2008, *ApJ*, 672, 371

Sakai, N., Saruwatari, O., Sakai, T., Takano, S., & Yamamoto, S. 2010, *A&A*, 512, A31

Sakai, N., Takano, S., Sakai, T., et al. 2013, *Journal of Physical Chemistry A*, 117, 9831

Sakai, N., & Yamamoto, S. 2013, *Chemical Reviews*, 113, 8981

- Sakaizumi, T., Katoh, F., Ohashi, O., & Yamaguchi, I. 1993a, *Journal of Molecular Spectroscopy*, 159, 112
- . 1993b, *Journal of Molecular Spectroscopy*, 159, 112
- Sakaizumi, T., Kikuchi, H., Ohashi, O., & Yamaguchi, I. 1987, *Bulletin of the Chemical Society of Japan*, 60, 3903
- Shimonishi, T., Das, A., Sakai, N., et al. 2020, *ApJ*, 891, 164
- Shingledecker, C. N., Lee, K. L. K., Wandishin, J. T., et al. 2021, *A&A*, 652, L12
- Sita, M. L., Changala, P. B., Xue, C., et al. 2022, *ApJL*, 938, L12
- Snyder, L. E., Hollis, J. M., Jewell, P. R., Lovas, F. J., & Remijan, A. 2006, *ApJ*, 647, 412
- Souza, S. P., & Lutz, B. L. 1977, *ApJL*, 216, L49
- Spezzano, S., Bizzocchi, L., Caselli, P., Harju, J., & Brünken, S. 2016, *A&A*, 592, L11
- Spezzano, S., Caselli, P., Pineda, J. E., et al. 2020, *A&A*, 643, A60
- Su, T., & Chesnavich, W. J. 1982, *Journal of Chemical Physics*, 76, 5183
- Suzuki, H. 1983, *ApJ*, 272, 579
- Suzuki, H., Ohishi, M., Kaifu, N., Ishikawa, S.-I., & Kasuga, T. 1986, *pasj*, 38, 911
- Suzuki, H., Yamamoto, S., Ohishi, M., et al. 1992, *ApJ*, 392, 551
- Takagi, N., Fukuzawa, K., Osamura, Y., & Schaefer, Henry F., I. 1999, *ApJ*, 525, 791
- Takano, S., Suzuki, H., Ohishi, M., et al. 1990, *ApJL*, 361, L15
- Takano, S., Masuda, A., Hirahara, Y., et al. 1998, *A&A*, 329, 1156
- Taniguchi, K., Herbst, E., Caselli, P., et al. 2019a, *ApJ*, 881, 57
- Taniguchi, K., Herbst, E., Ozeki, H., & Saito, M. 2019b, *ApJ*, 884, 167
- Taniguchi, K., Ozeki, H., & Saito, M. 2017a, *ApJ*, 846, 46
- Taniguchi, K., Ozeki, H., Saito, M., et al. 2016a, *ApJ*, 817, 147
- Taniguchi, K., Saito, M., & Ozeki, H. 2016b, *ApJ*, 830, 106
- Taniguchi, K., Saito, M., Sridharan, T. K., & Minamidani, T. 2018a, *ApJ*, 854, 133
- . 2019c, *ApJ*, 872, 154
- Taniguchi, K., Saito, M., Hirota, T., et al. 2017b, *ApJ*, 844, 68
- Taniguchi, K., Saito, M., Majumdar, L., et al. 2018b, *ApJ*, 866, 150
- Taniguchi, K., Herbst, E., Majumdar, L., et al. 2021, *ApJ*, 908, 100
- Taniguchi, K., Tanaka, K. E. I., Zhang, Y., et al. 2022, *ApJ*, 931, 99
- Taniguchi, K., Majumdar, L., Caselli, P., et al. 2023, *ApJS*, 267, 4
- Thaddeus, P., Gottlieb, C. A., Gupta, H., et al. 2008, *ApJ*, 677, 1132
- Thaddeus, P., Gottlieb, C. A., Hjalmarsen, A., et al. 1985a, *ApJL*, 294, L49
- Thaddeus, P., Vrtilik, J. M., & Gottlieb, C. A. 1985b, *ApJL*, 299, L63

- Travers, M. J., McCarthy, M. C., Gottlieb, C. A., & Thaddeus, P. 1997, *ApJL*, 483, L135
- Tucker, K. D., Kutner, M. L., & Thaddeus, P. 1974, *ApJL*, 193, L115
- Turner, B. E. 1971, *ApJL*, 163, L35
- Tychoniec, L., van Dishoeck, E. F., van't Hoff, M. L. R., et al. 2021, *A&A*, 655, A65
- Tyler, J. K., & Sheridan, J. 1963, *Transactions of the Faraday Society*, 59, 2661
- Villadsen, T., Ligterink, N. F. W., & Andersen, M. 2022, *A&A*, 666, A45
- Žabka, J., Ndiaye, I., Alcaraz, C., Romanzin, C., & Polášek, M. 2014, *International Journal of Mass Spectrometry*, 367, 1
- Wakelam, V., Loison, J. C., Mereau, R., & Ruaud, M. 2017, *Molecular Astrophysics*, 6, 22
- Walsh, C., Harada, N., Herbst, E., & Millar, T. J. 2009, *ApJ*, 700, 752
- Wang, S., Li, J., Guo, X., Jiang, L., & Zhang, J. 2009, *Journal of Molecular Structure: THEOCHEM*, 900, 118
- Watanabe, N., & Kouchi, A. 2002, *ApJL*, 571, L173
- Welty, D. E., Howk, J. C., Lehner, N., & Black, J. H. 2013, *Monthly Notices of the Royal Astronomical Society*, 428, 1107
- Winnewisser, G., & Walmsley, C. M. 1978, *A&A*, 70, L37
- Wohlfart, K., Schnell, M., Grabow, J.-U., & Küpper, J. 2008, *Journal of Molecular Spectroscopy*, 247, 119
- Woon, D. E. 1996, *ApJ*, 456, 602
- Woon, D. E., & Herbst, E. 2009, *ApJS*, 185, 273
- Xue, C., Willis, E. R., Loomis, R. A., et al. 2020, *ApJL*, 900, L9
- Yamamoto, S., Saito, S., Kawaguchi, K., et al. 1987, *ApJL*, 317, L119
- Zhang, Y., Higuchi, A. E., Sakai, N., et al. 2018, *ApJ*, 864, 76